MECHANISMS OF ADSORPTION OF AROMATIC NITROGEN COMPOUNDS AND AROMATIC HYDROCARBONS ON METAL-ORGANIC FRAMEWORKS (MOFs)

by

JUN DAI

A thesis submitted to the

Graduate School-Camden

Rutgers, The State University of New Jersey

in partial fulfillment of the requirements

for the degree of

Master of Science

Graduate Program in Chemistry

written under the direction of

Dr. ALEXANDER SAMOKHVALOV

and approved by

_____

Alexander Samokhvalov

_____

Alex J. Roche

_____

George Kumi

Camden, New Jersey

September 2014

THESIS ABSTRACT

MECHANISMS OF ADSORPTION OF AROMATIC NITROGEN COMPOUNDS AND AROMATIC HYDROCARBONS ON METAL-ORGANIC FRAMEWORKS (MOFs)

By JUN DAI

Thesis Director:

Professor ALEXANDER SAMOKHVALOV

Metal-Organic Frameworks (MOFs) constitute a class of novel porous materials that have attracted significant interest due to their applications in separation, storage, catalysis and chemical sensing. Their large surface area and highly porous structure make these materials excellent absorbents with a huge uptake capacity for many adsorbates of interest. Using complementary spectroscopic methods, we studied the mechanisms of adsorption of representative fused-ring aromatic compounds, namely indole and naphthalene, on the following MOFs: Basolite F300, MIL-100(Fe) and Basolite A100. Fluorescence spectroscopy and near-UV/Visible diffuse reflectance spectroscopy (near-UV-Vis DRS) studies demonstrate that naphthalene is confined within the mesocavity of F300 MOF. Moreover, we detected coordination bonds between adsorbed indole and F300 when indole was weakly electronically bound to Fe (III) CUS in F300 and MIL-100(Fe). Direct spectroscopic proof of the formation of an adsorption complex of indole with F300 and MIL-100(Fe) MOFs was obtained by near-UV-Vis DRS, wavelength-

dependent fluorescence spectroscopy, and complementary time-dependent fluorescence spectroscopy.

We have also determined the origin of the UV-Vis fluorescence in A100 MOF. We show that this fluorescence comes from the 1,4-benzenedicarboxylic acid (BDC) linker. The A100 MOF forms stoichiometric adsorption complexes with both indole and naphthalene. In these adsorption complexes, quenching of the ligand-based fluorescence from the BDC linker by the indole adsorbate was found. Based on wavelength-dependent fluorescence spectroscopy, we propose the adsorption of indole and naphthalene onto A100 MOF occurs via π-π interactions with the BDC linker.

Acknowledgements and Dedication

I would like to express my gratitude to Dr. Alexander Samokhvalov, who was my M.S. thesis advisor, for ideas and guidance throughout this entire thesis. I also thank Dr. Alexander Samokhvalov for supervising my research and the article successfully published following our joint efforts. I would also like to thank my M.S. Committee members: Dr. Alex J. Roche and Dr. George Kumi for their help with reviewing my thesis and their advice on my research. I thank the faculty, staff members, and fellow graduate students in Chemistry Department whom I had the pleasure to work with during my Graduate studies at Rutgers University. I also thank Dr. Jing Li who has synthesized an important material MIL-100(Fe) for our research.

Table of Contents

List of Figures

List of Tables

1 Introduction

1.1 Metal Organic Frameworks (MOFs)

Porous materials are being extensively studied and widely used in the science and engineering industry. Recently, a novel kind of porous material, Metal-Organic Frameworks (MOFs), has emerged. MOFs are crystalline hybrid inorganic-organic porous solids formed by metal cations connected to organic linkers [1]. The MOFs constitute a class of novel porous materials that have attracted significant interest due to their application in separation [2], storage [2], catalyst [2], and chemical sensing [3]. The use of MOFs as a stationary phase in high resolution gas chromatography (GC) separations of aromatic hydrocarbons has also gained significant attention [4]. While the adsorption of gaseous molecules onto MOFs has been well-studied [5–8], the adsorption of liquid phase molecules onto MOFs is poorly understood.

MOFs have an extremely large surface area and porosity, and this makes them excellent adsorbents for many adsorbates that are academically and industrially important. MOFs have their cavity size between that of zeolites and mesoporous silica [9], and they can display either two-dimensional or three-dimensional structures depending on the organic linkers and metals present. It was also indicated by Karra and Walton that the relation between pore size and guest molecule size plays an essential role in the adsorption process [10]. The MOFs investigated in this research were a group of representative mesoporous and microporous MOFs. For mesoporous MOFs, the pore size can vary from 2 nm to 50 nm, while for microporous MOFs the pore size is less than 2 nm. Pore size can be a key parameter in adsorption onto MOFs due to the micropore filling mechanism [4], which suggests that adsorption capacity depends on molecular cross-

sectional area rather than on the minimum molecular diameter. Many MOFs are structurally stable under ambient environment. It has been reported that certain MOFs remain stable under elevated temperatures in air or oxygen [11–13]. In this research, our investigation focuses on MIL-100(Fe) (MIL = Materials of Institute Lavoisier) and commercially available MOFs Basolite F300 and Basolite A100. Table 1 shows some basic physical information of the MOFs used in this research.

Table 1. The MOFs used in this research and structural information.

MOFs	The BET surface area, $m^2 g^{-1}$	Pore dimension, Å	Pore dimensionality	Ref.
Basolite F300	1300-1600	21.7	3D	Thierry *et al.* [12], Amarajothi *et al.* [14]
Basolite A100	1100-1500	7.3x7.7	1D	Thierry *et al.* [12]
MIL-100(Fe)	2200	25, 29	3D	Amarajothi *et al.* [14]

1.1.1 The MIL-100 family

MIL-100(M) (M=Cr, Fe, Al) refers to a family of mesoporous MOFs built up from metal clusters and linkers of 1,3,5-benzenetricarboxylic acid (BTC). The coordinatively unsaturated metal sites (CUS) in these MOFs cause Lewis acid-base interactions between guest molecules and metal ions or clusters in MOFs. These CUS are very important in gas storage, separation, sensing, catalysts, and even in the applications

for biological systems [15]. It was reported that Cu^{2+} CUS in HKUST-1 contribute significantly to the high acetylene storage capacity [16]. Moreover, MOFs with CUS, such as HKUST-1, were used in chromatographic separations due to their specific ability to distinguish between strongly and weakly electron donating analytes [6]. In addition, MIL-100 (Fe^{3+}, Cr^{3+}, Al^{3+}) have been shown to have a strong preference for N-heterocyclic compounds (that are Lewis bases) in solution [17,18]. Hence, CUS can function as Lewis acid sites for adsorption, and the possible interactions between guest molecules and CUS metal sites will be examined and discussed further.

In our research, MIL-100(Fe) will be used to investigate the adsorption mechanisms between benchmark fused-ring guest molecules, namely indole and naphthalene, and various MOFs. Besides MIL-100, there is a commercially made MOF termed Basolite F300, which has a similar chemical composition [14]. Both Basolite F300 and MIL-100(Fe) consist of iron sites and BTC linkers, although some details of the structure of F300 are still not known. The difference in iron content and carbon content in F300 and MIL-100 (Fe) was found by Amarajothi and co-workers [14]. Specifically, the iron content in F300 and MIL-100 (Fe) is 25 wt. % and 21 wt. %, respectively. The carbon content in F300 and MIL-100 (Fe) is 32 wt. % and 29 wt. %, respectively. Pore dimensions in F300 and MIL-100 (Fe) are 21.7 Å, and 25 and 29 Å (two mesocavities), respectively [14]. The structure of MIL-100 (Fe) is shown in the supplementary Figure 1.

Figure 1: Structure of MIL-100(Fe) (see as S1 in the Supplementary)

1.1.2 The MIL-53 family

There are many types of MOFs that undergo hydrolysis, while there are some MOFs that remain stable in liquid or gaseous water. The water stable MOFs have started to show various potential applications in water adsorption [19], drug delivery and imaging [20]. Many MOFs containing Al as metal sites and amino acids as organic linkers are stable in aqueous solutions, and it is also possible to synthesize them in aqueous environment [21]. MIL-53(M) (with M = metal such as Al [12], Cr [22], Fe [23], In [19], and Sc [24]) is a well-known family of microporous MOFs, and many MIL-53 MOFs have an excellent water stability [25,26]. The three-dimensional structure of MIL-53(Cr) illustrating different hydrated structures is shown in the Figure 2.

Figure 2: Structure of MIL-53 MOF (Cr) (see as S2 in the Supplementary)

The one-dimensional pore structure of MIL-53(Al) is made up of chains of corner-sharing octahedral clusters $AlO_4(OH)_2$ linked by the dianionic form of benzene-1,4-dicarboxylic acid (BDC). MIL-53(Al) has rhombic channels [12] with dimensions of 7.3 by 7.7 Å. A huge Langmuir surface area of 1600 m^2/g makes MIL-53(Al) an efficient adsorbent. MIL-53(Al) has an extraordinary thermal stability [27] up to 723 K. The structure of MIL-53(Al) undergoes a reversible structural change during the process of adsorbing/desorbing water molecules that is termed “breathing” [12]. This so-called “breathing” process causes an interchange between the large-pore (*lp*) form of MIL-

53(Al), (Al(OH)[O_2C-C_6H_4-CO_2]) and the narrow-pore [12] (*np*) form Al(OH)[O_2C-C_6H_4-CO_2] ·H_2O. The (*lp*) form of MIL-53(Al) has a pore dimension of 8.5 by 8.5 Å, and it is obtained when MIL-53(Al) is activated at high temperature in the high vacuum, which removes an excess of free BDC acid, adsorbed oxygen and water trapped in the cavities from the synthesis of the MOF. The (*lp*) form is capable of adsorbing water molecules in vapor at room temperature, and as a result, MIL-53(Al) changes to its (*np*) form.

The (*np*) form contains one trapped water molecule per every structural unit or the microcavity (Figure 2). Hydrogen bonds are found to form between carboxylic groups of the BDC linker and adsorbed water molecules [12]. Due to the "breathing" feature, applications of selective adsorption of various compounds in the gas phase have already gained interest and have being reported [22]. The (*np*) form of hydrated MIL-53(Cr) is able to selectively adsorb CO_2 in the presence of CH_4 in the gas phase [22]. Upon this selective adsorption of CO_2, MIL-53(Cr) returns to its (*lp*) form with an increased cavity volume of 1522.5 $Å^3$ compared to that of (*np*) form at 1012.8 $Å^3$.

In our research, we used Basolite A100 MOF which is commercially available from the BASF and that is similar to MIL-53(Al). A100 is made out of $AlO_4(OH)_2$ octahedral clusters connected by BDC linkers. A100 has a surface area of 1084 m^2/g and pore volume of 0.51 cm^3/g as was determined by N_2 physical-adsorption at 77 K [28]. Additionally, the powder XRD pattern of A100 resembles that of MIL-53 (Al) [28]. Blanco-Brieva *et al.* have studied an adsorptive removal of aromatic sulfur compounds from model liquid fuels on thermally activated A100 MOF [29].

1.2 Clean Fossil Fuels

Fossil fuel is a primary source of energy on the earth, and the intensive use of fossil fuels has raised significant environmental concerns. Combustion of sulfur and aromatic N-heterocyclic compounds present in fossil fuels brings adverse consequences to public health, environment and economy. Many studies have shown that air pollutants can be carcinogenic and mutagenic [30,31]. Beginning in 2006, the Environmental Protection Agency (EPA) in the U.S. began an ambitious program aimed at reducing the sulfur content of diesel fuel. As of 2010, the EPA has required that the concentration of sulfur content in diesel fuels be less than 15 ppm [32]. For certain ultra-clean gasolines, diesel fuels and jet fuels, sulfur levels need to be lower than 1 ppm [33].

The separation of heterocyclic compounds from petro-chemical feedstock has become an important issue in the manufacture of clean liquid fossil fuels. Hydrodesulfurization (HDS) of diesel fuel has become an essential interest, while the presence of aromatic N-heterocyclic compounds in middle-distillate oil inhibits ultra-deep HDS [34–37]. In HDS, sulfur compounds are catalytically hydrogenated to hydrocarbons and H_2S [17]. However, aromatic N-heterocyclic compounds present in crude oil are found to compete for the active sites on these catalysts, and thus these aromatic compounds inhibit a deep HDS [38,39]. This gives rise to the necessity for denitrogenation of fossil fuels by alternative methods.

The combustion of aromatic N-heterocyclic compounds present in fuels leads to production of nitrogen oxides that form a group of highly reactive and persistent species, and these species contribute directly to acid rain and the greenhouse effect. The life time of N_2O in the atmosphere is ca. 120 years before it is removed or destroyed through

chemical reactions [40]. The impact of 1 pound of NO_x on warming the atmosphere is over 300 times that of 1 pound of carbon dioxide. The U.S. EPA established the first standard for NO_2 in 1971, setting both a primary standard (to protect health) and a secondary standard (to protect the public welfare) at 0.053 parts per million (53 ppb) averaged annually [41]. Also, the presence of aromatic N-heterocyclic compounds in fossil fuels can lead to the poisoning of catalysts used at petroleum refineries, and this poisoning can eventually cause a decrease in the fuel yield. Thus, denitrogenation is necessary for the deep desulfurization and production of clean fuels, and it has drawn significant interest around the world because of the increasingly rigid regulations and fuel specifications in many countries.

1.3 Aromatic N-heterocyclic Compounds in Fossil fuels

Fossils are naturally-formed deposits that contain significant amounts of heterocyclic aromatic contaminants. One usually considers the representative aromatic S-heterocyclic compounds present in fossils, e.g. benzothiophene (BT) and dibenzothiophene (DBT), and the representative aromatic N-heterocyclic compounds, such as indole and quinoline. The content of aromatic N-heterocyclic compounds in crude oil averages at ca. 0.3 % [42]. Although the concentration of aromatic N-heterocyclic compounds in crude oil is relatively low, the concentration progressively increases through the petroleum distillation and catalytic reforming process. The common aromatic N-heterocyclic compounds present in fossil fuels are shown in Figure 3, and their physical properties of relevance to this research are shown in Table 2.

Aromatic N-heterocyclic compounds in fossil fuels belong to two major classes. One is the group of non-basic N-heterocyclic compounds, including indole and pyrrole,

where the pair of electrons on the N atom contributes to the π-electron system of an aromatic ring. Thus, this electron is not available for interaction with acids. The other class is the set of basic N-heterocyclic compounds such as pyridine, quinoline and their derivatives, in which the lone pair of electrons on N atom is available for the interactions with Brønsted or Lewis acids.

Indole is one of the most common N-heterocyclic compounds present in fossil fuels. We have chosen indole for our research due to the fact that indole is a weakly basic N-heterocyclic compound, which means that it has a potential of being selective adsorbed compared to other aromatic compounds. Furthermore, its subsequent desorption is possible.

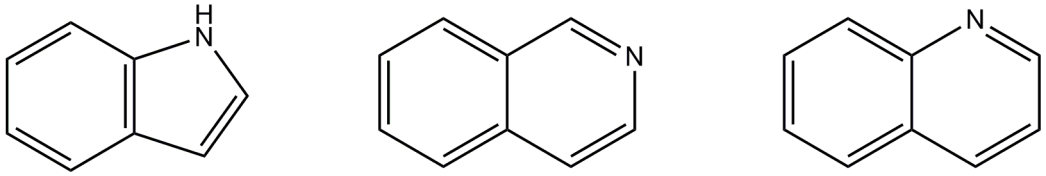

Indole Isoquinoline Quinoline

Figure 3: Common aromatic N-heterocyclic compounds present in fossil fuels.

Table 2. Physical properties of common N-heterocyclic compounds in fossil fuels.

Compound	Formula	Melting Point, ℃	Density, g/cm^3	Dipole moment, D	Acidity, pK_a	Maximum diameter, ˚A
Indole	C_8H_7N	52-54	1.17	2.11	16.2	6.9
Quinoline	C_9H_7N	-15	1.093	0	4.85	7.2
Isoquinoline	C_9H_7N	26-28	1.099	0	5.14	7.2

1.4 Aromatic Compounds in Fossil Fuels

Fossil fuels contain a significant amount of hydrocarbons, most of which are polycyclic aromatic hydrocarbons (PAHs). In this research, we chose naphthalene as a representative fused-ring aromatic compound. In order to investigate the adsorption mechanism of naphthalene, we used fluorescence spectroscopy and UV-Vis diffuse reflectance spectroscopy (near-UV-Vis DRS) to investigate electronic interactions upon adsorption onto MOFs. Naphthalene is the most simple and common aromatic compounds among the PAHs, and naphthalene is abundantly present in the streams of petroleum refinery and commercial liquid fuels. Thus, the separation and purification of fused-ring PAHs, e.g., naphthalene, is of interest to the chemical industry. Naphthalene has a molecular length of 7.2 Å (the largest diameter as determined by ChemDraw 3D), and is non-polar.

1.5 Methods of Denitrogenation

1.5.1 Microbial Denitrogenation

Microbial processing is an alternative pathway for denitrogenation of liquid fuels. Microorganisms are known to consume natural organic compounds and convert them into carbon and energy, and they are capable of metabolizing certain molecules including aromatic N-heterocyclic compounds from fossil fuels. The degradation of quinoline is well-characterized, and the transformation pathways are elucidated by Benedik *et al.* [42] (shown in Figure 4). The degradation of isoquinoline is less understood, but 1-oxo-1,2-dihydroisoquinoline is suggested as the initial oxygenated product [43]. According to the finding of Claus [43], indole is readily degraded via catechol or transformed directly into tryptophan, while carbazole is relatively more difficult to degrade. One possible

degradation pathway has been proposed by Ouchiyama [44]. In this process, carbazole is first dioxygenated to form 2'-aminophenyl-2,3,-diol, then degrades through *meta* cleavage of the diol ring to form 2-hydroxy-6-oxo-6-(2'-aminophenyl)hexa-2,4-dienoic acid. After further hydrolysis, 2-hydroxy-4-pentenoate and anthranilic acid are formed , and finally enters the central metabolic pathway tricarboxylic acid cycle (TCA cycle) [45]. The mechanisms for the degradation of other N-heterocyclic compounds such as pyridine, quinoline, acridine and their derivatives are reviewed in detail by Kaiser [46]. However, with respect to the removal and metabolism of organic compounds from the environment, characterization of enzyme-involving pathways is still under research [42]. Indeed, microbial denitrogenation has not been applied in industry yet.

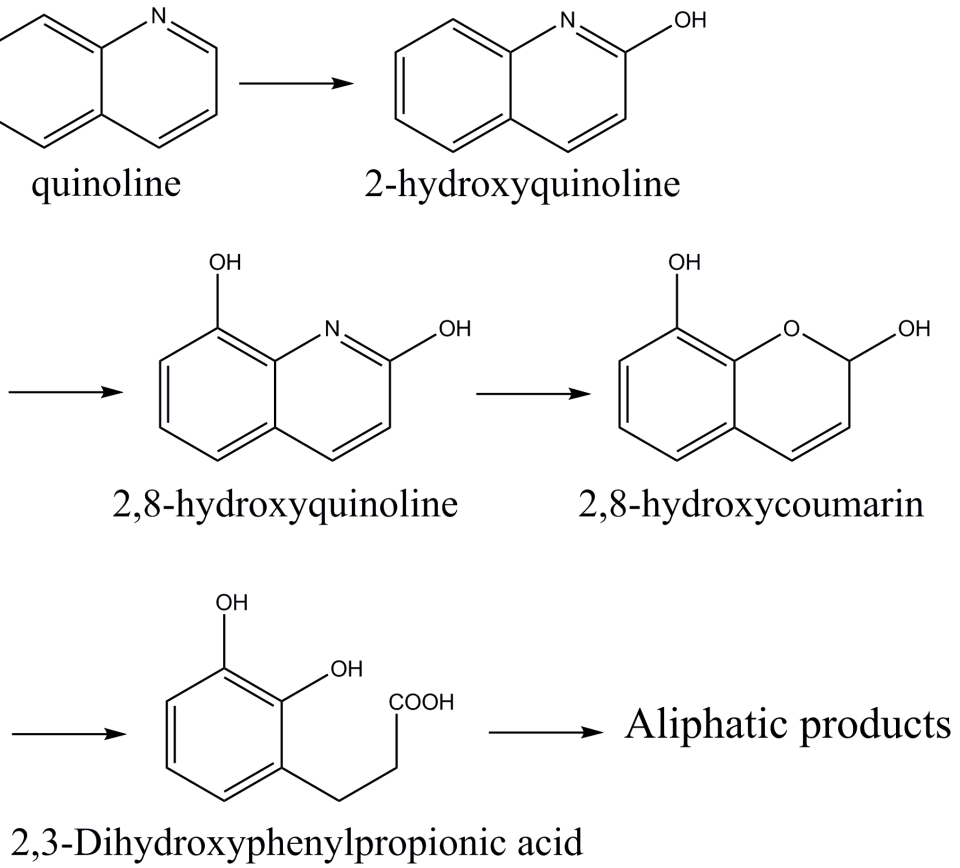

Figure 4. Pathways for the transformation of quinoline.

1.5.2 Hydrodenitrogenation (HDN)

Hydrodenitrogenation (HDN) is usually used to catalytically remove aromatic N-heterocyclic compounds from fossil fuels during refinery processing, and a catalyst is normally required [47]. However, the HDN process is conducted by reacting refinery streams with hydrogen at high temperature and high pressure. This procedure is energy-intensive, hazardous and costly. Thus, a significant amount of research has been done on the HDN in order to reach a goal of being economic and environmentally friendly [47–49].

1.5.3 Adsorptive Denitrogenation (ADN)

Another promising way to selectively remove aromatic N-heterocyclic compounds present in fossil fuels is by adsorbing them onto a suitable porous material. Specifically, activated carbon [50–53], zeolites [54], HCl-loaded silica-aluminas [55], ion-exchange resins [56], meso-silicas [57,58], Ti-hexagonal mesoporous silicates (Ti-HMSs) [59], microporous carbon [60], activated aluminas [61], Ni-based adsorbents [61], and NiMoS catalyst [62] have been used for the ADN. Due to the high capacity, selectivity, economic importance, and most importantly, potential energy savings, research on MOF has gained significant interest recently for the adsorption and separation of aromatic and heterocyclic compounds in the liquid phase [63]. Moreover, MOF sorbents can be recycled, and this effectively reduces the cost of the expected technological process. Adsorptive separation via the ADN is preferred over industrial catalytic HDN [18]. Specifically, selective adsorption of N-heterocyclic compounds [64] in the liquid phase in the presence of aromatic and aliphatic hydrocarbons [65] is of interest in our research.

1.6 Activation of Open Metal Sites of Metal-Organic Frameworks

The presence of CUS in MOFs is essential for the adsorption of chemical compounds with Lewis basicity. Thus, to fully utilize the CUS in MOF sorbents, activation is needed to 1) evacuate the water molecules which are relatively weakly coordinated on the CUS and 2) remove any excess of the linker-forming organic precursor remaining from the synthesis of the MOFs. Because MOFs have a high adsorption capacity for many potential adsorbates, humidity can be crucial for the availability of CUS in MOFs. Specific treatment is necessary in order to activate the CUS, and the protection of the sample against humidity is critical during the experiments. Interestingly, it was discovered by Schlichte *et al.* [11] that upon thermal activation, the color of HKUST-1 changes from light cyan to dark navy. This is confirmed by Borfecchia *et al.* [7] using UV-Vis DRS spectroscopy via the red shift of the edge of the Ligand to Metal Charge Transfer (LMCT) band, and the appearance of a shoulder in the d-d band at about 600 nm, as explained by the removal of water from the Cu^{2+} CUS.

In addition to the activation of the MOFs, partial reduction of MIL-100(Fe) has been reported by Leclerc *et al.* [66]. Certain metal sites in the MOFs can be reduced, for example, Fe^{3+} in MIL-100(Fe) can be reduced to Fe^{2+} [2]. According to the analysis of oxidation states by the Fourier Transform Infrared Spectroscopy (FTIR), outgassing at 423 K for 12 hours gives rise to a higher proportion of Fe^{2+} sites, while the Fe^{3+} sites are reduced. However, outgassing at 523 K results in the majority of Fe^{3+} being reduced. The Fe^{3+} sites are harder Lewis acidic sites than Fe^{2+}, and thus it is easier for Fe^{3+} to form coordination bonds with aromatic N-heterocyclic compounds, which are the strong Lewis bases [2].

1.7 Adsorption of Aromatic Compounds and Aromatic N-heterocyclic Compounds on mesoporous MOFs with CUS: MIL-100 (Fe) and F300

Although the adsorption of small organic molecules on MOFs, both in the liquid phase and in vapor, has been studied in recent years, the adsorption of fused-ring aromatic hydrocarbons on MIL-100 in the liquid phase has not been reported, to our knowledge. Maes *et al*. reported an adsorption of indole from a heptane/toluene mixture on the MOFs of the MIL-100 family [17]. However, the mechanism of adsorption of aromatic compounds versus aromatic N-heterocyclic compounds on MIL-100(Fe) or F300 MOF has not been studied. According to many studies [2,17,18], the formation of adsorption complexes during adsorption in the liquid phase is usually assumed, but there is a lack of direct spectroscopic evidence. Adsorption of small-ring aromatic compounds (e.g., benzene and isomeric p-xylene molecules) on MIL-101 has been published by Yang *et al* [4]. The pore-size filling mechanism was discovered and discussed in this paper with the notion that pore size and the structure of the isomeric adsorbate affects the adsorption capacity. However, the mechanism of adsorption is still not understood and has not been proven spectroscopically.

Fluorescence spectroscopy is a straightforward method for studying the adsorption mechanism between the aromatic and heterocyclic "guest" molecules and MOF sorbents. Yet, there are rarely papers that report the characterization of the adsorption of aromatic compounds in the liquid or solid system using fluorescence spectroscopy. Based on fluorescence spectra, it was assumed that a Lewis acid-base interaction promotes the adsorption of pyrene on Al_2O_3 from model fuel [67]. However, these fluorescence spectra were collected using a model sorbent aluminum chloride in methanol, rather than Al_2O_3.

Thus, the adsorption mechanism with alumina sorbent was not directly studied. The spectroscopic characterization of adsorption complexes formed by MOFs and aromatic compounds or aromatic N-heterocyclic compounds by fluorescence spectroscopy has not been reported, to our knowledge.

Another useful characterization method is near-UV/visible diffuse reflectance spectroscopy (near-UV-Vis DRS), which is excellent at detecting the variation or shift in the electronic states in the adsorption complexes formed by metal sites and guest molecules. Near-UV-Vis DRS was used to identify the interactions between aromatic amines and MOFs [68], but it has not been used to explore the interactions between metal sites in the MOFs and guest molecules that are aromatic hydrocarbons or aromatic N-heterocyclic compounds.

Thus, we aim to investigate the adsorption of the representative aromatic N-heterocyclic compounds and aromatic hydrocarbons on MOFs with and without the CUS, using two complementary spectroscopic methods: fluorescence spectroscopy and near-UV/visible diffuse reflectance spectroscopy.

1.8 Adsorption of Aromatic Compounds and Aromatic N-heterocyclic compounds on microporous MOFs without CUS: MIL-53 and A100

Maes *et al*. studied the adsorption of indole and methyl-substituted indole present in model fuel at an initial concentration of 0.15 M on thermally activated MIL-53 (Al) [17]. The solvent was a mixture of heptane/toluene at either 80 vol. %/20 vol. % or 20 vol. %/80 vol. %, respectively. The amount of absorbed indole strongly decreased in the model fuel with the higher content of toluene, which indicates a possible competitive adsorption of toluene with indole. There is no experimental evidence of the mechanism of

competitive adsorption of aromatic hydrocarbons *vs*. N-heterocyclic compounds on any MOFs.

Similarly, adsorption of indole, pyridine, pyrrole and quinoline on thermally activated MIL-53(Al) was studied recently [69], and n-octane was used as solvent. However, no data on the adsorption capacity of MIL-53(Al) for indole was reported. Also, although it was suggested that π-π interactions are the major mechanism of adsorption of indole or quinoline on the activated MIL-53(Al), no experimental evidence was provided [69]. At present, no direct spectroscopic characterization of chemical bonds between the aromatic or heteroaromatic adsorbate and adsorption sites in the MIL-53 MOFs has been reported. Furthermore, the adsorption of naphthalene on MOFs has not been reported, to our knowledge.

To investigate adsorption mechanisms involving MOFs using fluorescence spectroscopy, it is essential to know the origin of the fluorescence from the MOF itself. It was discussed in a review paper by Allendorf *et al*. [70], that there are five possible fluorescence mechanisms in the MOFs, namely fluorescence i) from the linker, ii) from metal ions, iii) due to the charge transfer between the ligand and metal, namely Ligand to Metal Charge Transfer and Metal to Ligand Charge Transfer (LMCT and MLCT), iv) due to adsorbed lumophores, and v) due to the exciplex formation (π-π interaction). Both F300 and MIL-100 (Fe) are weakly fluorescent MOFs. However, it was speculated that an emission from MIL-53(Al) at ca. 410 nm may originate from the LMCT [71,25]. Yet, no evidence was provided to prove whether the LMCT is responsible for the fluorescence of MIL-53(Al). Also, very few reports on the characterization of adsorption of aromatic compounds on metal oxide by the fluorescence spectroscopy are available [67]. The direct

experimental determination of the chemical bonding in the “host-guest” adsorption complexes of the MOFs and aromatic compounds or aromatic N-heterocyclic compounds using the fluorescence spectroscopy or other spectroscopic methods has not yet been reported.

1.9 Research Objective

The general objective of this research was to investigate the mechanisms of adsorption and desorption of the representative fused-ring aromatic N-heterocyclic compound and aromatic hydrocarbon on the representative microporous MOF (without CUS) and mesoporous MOFs (with CUS). Our first specific objective was to investigate the similarities and differences in chemical bonding of the simplest fused-ring aromatic N-heterocyclic compound indole and fused-ring aromatic hydrocarbon naphthalene to the F300 MOF, which has CUS. The second specific objective was to investigate the similarities and differences in chemical bonding of indole and naphthalene to MIL-100(Fe) and F300 MOF. The third specific objective was to investigate chemical interactions of indole and naphthalene with the microporous MOF A100, which does not have CUS.

2 Experimental

2.1 Metal Organic Frameworks

Basolite F300 and Basolite A100 were bought from Sigma Aldrich, and MIL-100(Fe) was supplied by our collaborator Dr. Jing Li from Rutgers – New Brunswick.

2.2 Solvents, aromatic compounds and aromatic N-heterocyclic compounds

The solvents used in this research are dimethylformamide (DMF), n-hexane, n-heptane, n-tetradecane, pH 8.5 sodium phosphate buffer solution and eicosane. Organic compounds used in this research are naphthalene, indole, 1,3,5-benzenetricarboxylic acid (BTC), and benzene-1,4-dicarboxylic acid (BDC). Eicosane, pH 8.5 buffer solution, n-hexane, indole, benzene-1,3,5-tricarboxylic acid and benzene-1,4-dicarboxylic acid were bought from Sigma-Aldrich and used as received. Naphthalene and n-heptane were bought from Acros Organics and used as received. Dimethylformamide and tetradecane were from TCI Inc.

2.3 Activation and Hydration of Metal-Organic Frameworks

All MOFs were bought in their *as-synthesized* form, i.e. in the non-activated form, with water and free organic ligand remaining from the synthesis of the MOF. An activation of the MOFs is necessary before studying the adsorption of "guest molecules". The activation of the MOFs is mostly desorption of water, oxygen and other impurities, such as free organic ligands remaining in the framework. The different MOFs require different activation processes.

The recommended activation procedures for both Basolite F300 [14] and A100 [27] have been reported. Moreover, the A100 MOF was shown to remain structurally stable at 603 K for 72 hours [27]. Based on finding by Schlichte [11], activation of Basolite F300 and

Basolite A100 in this research was conducted under high vacuum (<1 × 10^{-3} Torr) at temperature of 423 K for 24 hours.

For MIL-100, it was reported [2] that a variety of activation conditions can be adopted to give the different activated MOFs, and even a different ratio of Fe^{2+} /Fe^{3+} CUS. In our research, we activated MIL-100(Fe) under high vacuum at 423 K for 12 hours. According to the reference procedure, our activation process should give a high total amount of Fe^{3+} CUS and a small fraction of Fe^{2+} CUS.

The hydration of thermally activated MOFs was conducted in water vapor in a desiccator filled with liquid water, the MOF powders were placed on a tray above the water level, and the desiccator was closed. The hydration process takes 2 or 7 days depending on different hydration level, after which the MOF was taken out of the desiccator and placed into a sealed bottle with water vapors in order to maintain the same hydration conditions. The change in mass of the MOF after the hydration was determined gravimetrically.

2.4 Fluorescence Spectroscopy

Fluorescence Spectroscopy was conducted using a Cary Eclipse Fluorescence Spectrophotometer from Agilent Technologies Inc. The sample holder was a custom-made temperature-controlled cuvette holder (TLC) from Quantum Northwest that was designed to avoid spectral distortions caused by primary and secondary re-adsorption of light [72]. In order to improve the monochromaticity of the excitation light, narrow bandpass (5 or 10 nm) optical filters centered at different wavelengths (260, 280, 300, 310 and 372 nm) were used. The bandwidths of excitation and emission slits were 5 nm and 5 nm, 10 nm and 5 nm, or 20 nm and 5 nm, respectively, and were chosen based on

the intensity of the fluorescence. When the bandwidth of 2.5 nm for both slits was used, the better resolved spectrum with same shape but much lower intensity was obtained, as expected.

For datasets with multiple peaks, numeric curve-fitting of the fluorescence spectra was conducted using the Microcal Origin program. The built-in Local Maximum method was used to identify the peaks automatically with a straight baseline at Y=0. The Multiple-Gaussian fit option in Origin's peak analyzer was applied to fit the datasets into multiple peaks.

2.5 Near UV-Vis Diffuse Reflectance Spectroscopy (near UV-Vis DRS)

Diffuse Reflectance Spectra were measured using a UV-Vis spectrometer, with a xenon (LS-1) lamp as light source, a fiber-optic reflection probe, and a Diffuse Reflectance Standard (WS-1) from Ocean Optics.

2.6 Model Fuels

In this research, we used 0.08 M solution of indole (IND) in n-heptane and 0.08 M solution of naphthalene (NAP) in n-heptane. Each solution was prepared by the sonication of a calculated amount of aromatic compound in neat solvent at room temperature until complete dissolution. The concentration of 0.08 M was chosen 1) due to the fact that it is close to the maximum solubility of indole and 2) in order to achieve the maximum adsorption capacity on the MOFs. Moreover, this concentration is close to the total content of nitrogen present as aromatic N-heterocyclic compounds in certain petroleum refinery streams [73].

2.7 Solid Mixture of Aromatic and Aromatic N-heterocyclic compounds with MOFs

We prepared the solid mixture in the 0.5 cc quartz cuvette or 1.5 cc quartz cuvette. For the non-activated MOFs, the MOF was weighed in the cuvette, and the calculated amount of melted organic compound was added. The cuvette was closed with a PTFE stopper. After adding melted substances into the cuvette, the cuvette was well mixed until it slowly solidified while being continuously shaken at 298 K. This method was used to achieve an effective mixing of the MOF with the organic compound and to obtain a uniform solid mixture. For the activated MOFs, the MOF was first activated and then mixed with melted substances under argon, and the cuvette with the mixture was sealed. The samples were optically uniform and had a typical color of the MOFs used. Two sets of molar ratios were applied, which are R_1 = n(naphthalene)/n(F300) = n(indole)/n(F300) = 50 and R_2 = n(naphthalene)/n(F300) = n(indole)/n(F300) = 15 where n is the number of moles.

2.8 The stoichiometric adsorption complex of F300 and naphthalene in eicosane matrix

First, 85 mg of F300 was activated in a 1.5 cc quartz cuvette, and approximately 1.4 cc solution of 0.08 M naphthalene in eicosane ($C_{20}H_{42}$) was added when melted under argon. The cuvette was closed with a PTFE stopper and mixed well until fully solidified at 298 K. The solid solution of 0.08 M naphthalene in eicosane was prepared by adding the calculated amount of solid naphthalene into melted pure eicosane. Then the mixture was heated at 313 K on a sonic bath until complete dissolution. The solution was allowed to cool to room temperature during which it solidified. The sample with F300 MOF and naphthalene in eicosane matrix contained 0.11 mmol naphthalene and 0.33 mmol F300

(M.W. 263 g/mol for the Hill formula $C_9H_3FeO_6$) and, as a result, molar ratio of one molecule of naphthalene per three Fe cations in F300 was obtained.

2.9 Kinetics of adsorption of liquid indole on Basolite F300 in liquid phase

To investigate the formation of the complex of indole with F300 with Fe^{3+} CUS, we conducted a time dependent adsorption study of liquid indole on F300 MOF. We used time-dependent fluorescence spectroscopy to examine the adsorption kinetics. At first, 200 mg F300 was weighed in a 3.5 cc quartz cuvette and activated under vacuum at 423 K. After 24 hours, the cuvette was vented and mixed with 1.334 g melted indole under argon. Then the mixture was allowed to solidify immediately and was mounted onto the TLC accessory of Cary Eclipse which can rotate the PTFE-coated mini magnetic stir bar inside the cuvette. The cuvette with the mixture was heated up to constant temperature of 333 K that caused melting indole in the mixture to form a suspension of F300 MOF in melted indole, and was kept under stirring with a mini stir bar. The time-dependent fluorescence spectra from the suspension at 333 K were collected every 7 minutes at λ_{exc} = 310 nm.

2.10 The stoichiometric adsorption complexes of indole/naphthalene with MOFs

To investigate the formation of the stoichiometric “host-guest” adsorption complexes with the MOFs, we attempted to prepare the “pure” adsorption complexes of indole or naphthalene with F300, MIL-100 and A100. These “pure” complexes were made through the activation, mixing, adsorption, and evaporation of the solvent and any non-adsorbed compounds. At the beginning, we weighed the calculated amount of MOFs in the 0.5 cc quartz cuvette to reach an equimolar ratio of indole or naphthalene (one guest molecule per one metal site in the MOF). For F300 with indole or naphthalene, 28.6 mg F300 was

weighed. For A100 with indole or naphthalene, 24.3 mg A100 was weighed, and for MIL-100, 34.0 mg MIL-100 was weighed. The non-activated MOFs, activated MOFs or hydrated MOFs were used as needed. Approximately 0.4 cc of solution was added to the cuvette of the nominal volume of 0.5 cc under argon, the cuvette was nearly full to exclude air or moisture, and was closed with a PTFE stopper. After mixing with 0.4 cc 0.08 M solution of indole or naphthalene, the cuvette was mounted onto a mechanical shaker (Roto Shake Genie from Scientific Industries) and shaken at the maximum speed for 1 hour. After 1 hour, the cuvette was removed from the shaker and placed in a vessel which was connected through a valve to the high vacuum system. The valve was slowly opened to maintain the vacuum $<1 \times 10^{-1}$ Torr until the complete evaporation of the solvent was achieved. Then, the turbo pump was turned on and operated until the pressure decreased below 1×10^{-3} Torr to remove any non-adsorbed indole or naphthalene. Afterwards, the vacuum system was vented with argon to prevent any contamination of the obtained pure adsorption complexes from ambient humidity or other impurities. Finally, the pure complexes were obtained as dry powder in the cuvette that was sealed. The initial weights of the substances and the MOFs, and the final weight of the "pure complexes" were determined using an analytic balance from Fisher Scientific. Preparation of the samples and measuring their spectra were repeated three times.

2.11 Fluorescence under the UV lamp

To visualize the near-UV and visible fluorescence from the adsorption complexes of A100 MOF, we used a UV lamp (from Spectronics) to illuminate our samples at 254 nm or 312 nm. The samples were placed on a white paper against the black background in

the dark room, and digital photographs were taken. No digital image processing was performed.

3 Results

3.1 Spectroscopic studies of adsorption of naphthalene and indole on mesoporous F300 and MIL-100 (Fe) with CUS

3.1.1 Solid Mixtures of MOFs and organic aromatic compounds

To exclude possible artifacts, fluorescence spectra were collected from 1) the empty quartz fluorescence cuvette using the angular accessory and 2) the cuvette filled with n-heptane. In both cases, as expected, no fluorescence was detected. The adsorption spectrum of 5.4×10^{-4} M of naphthalene in n-hexane was reported [74] to have adsorption peaks at 218, 222, 286 and 320 nm. Those electronic transitions were confirmed by the adsorption and fluorescence spectra, as well as by quantum chemical calculations [74]. In our case, the fluorescence peaks at 218 and 222 nm would be rather difficult to obtain with the MOFs samples, due to the optical properties of the BTC linker and the quartz cuvette. In rather diluted 0.08 M solution of naphthalene in n-heptane, one naphthalene molecule is calculated to be surrounded by 82 molecules of n-heptane, on average. Therefore, naphthalene molecules are isolated from each other in this solution. Figure 5 shows the fluorescence spectrum of the 0.08 M solution of naphthalene in n-heptane obtained with λ_{exc} = 280 nm (both excitation and emission slits were 5 nm). There are 39 vibrational bands observed by O. Schnepp and D. S. Mcclure [75] in their measurement of naphthalene vapor. In our fluorescence measurement of naphthalene in liquid solution, five adsorption peaks are present in the spectrum, and their assignments to the vibronic components in the fluorescence spectra are shown: at 312 nm (0-0 transition), 323 nm (0-1), 335 nm (0-2), 350 nm (0-3), 368 nm (0-4 transition). This could be due to a rather diluted concentration in our experiment, and a higher resolution in the vapor phase

measurement than liquid phase measurement. And our spectrum corresponds well with the fluorescence data of naphthalene in cyclohexane [76]. In the reported fluorescence spectrum of naphthalene in solution [74], a weak band at 315 nm was assigned to the 0-0 transition, consistent with the fluorescence spectrum of a dilute solution of naphthalene in n-pentane at cryo-temperatures measured in Shpolskii matrix. In our case, we assigned the small shoulder at 312 nm in Figure 5 to the 0-0 transition based on the study by Privalova *et al.* [74] and references therein. The deviation of 3 nm from published value [74] can be due to an error in the determination of the peak center or instrument error. Also, our assignment of 312 nm peak is confirmed by a reported analysis of the fluorescence spectrum of naphthalene vapor under room temperature by Behlen *et al.* [77] in which the origin of $^1B_{3u}^- \leftarrow {}^1A_g^-$ transition was found at 32018.5 cm^{-1} (312 nm).

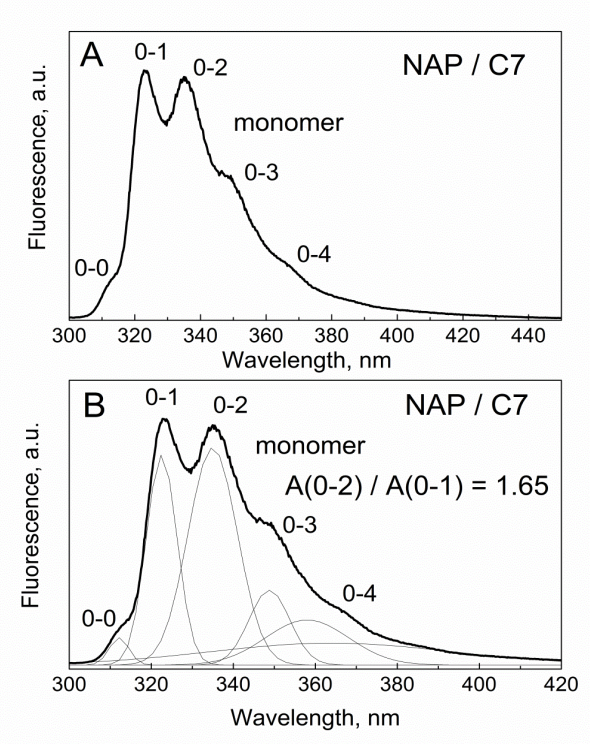

Figure 5: Fluorescence spectra of (A) 0.08 M liquid solution of naphthalene (NAP) in n-heptane at λ_{exc} = 280 nm; (B) 0.08 M liquid solution of NAP in n-heptane and its multi-Gaussian curve fitting.

The next adsorption peak at 323 nm (Figure 5) was also detected at 323 nm in the reported spectrum of naphthalene in n-hexane solution [74]. The peak at 323 nm was assigned by Privalova *et al.* [74] to the 0-1 transition coupled to the vibration of naphthalene at 506 cm^{-1} ($\upsilon_{01} = \upsilon_{00} - 506\ cm^{-1}$). Therefore, we assigned the peak at 323 nm to the same 0-1 vibronic transition. Further, the peak at 336 nm was assigned to the 0-2 transition in the reported spectrum [74] coupled with vibrations at 506 and 1,380 cm-1 ($\upsilon_{02} = \upsilon_{00} - 1{,}380 - 506\ cm^{-1}$). Moreover, we notice that the vibration at 506 cm^{-1} (in our measurement in solution, Figure 5) is intra-molecular vibration rather than the inter-molecular vibration (e.g. vibrations in a solid crystal of naphthalene [78]). Hence, it is reasonable to believe that this specific vibronic component in the fluorescence spectrum of naphthalene would be present in both the liquid and solid phase.

Furthermore, a shoulder at 350 nm in Figure 5 is consistent with the reported 0-3 transition coupled with collective vibrations ($\upsilon_{03} = \upsilon_{00} - 506\text{-}2 \times 1{,}380\ cm^{-1}$) [74]. The band at 368 nm in Figure 5 is a weak component and is absent in the fluorescence spectrum of solution of naphthalene in n-hexane [74]. This weakness in intensity is probably because the solution was very dilute. Nonetheless, the shoulder at 368 nm in Figure 5 can be interpreted as the next member of the vibronic multiplet of the fluorescence spectrum of naphthalene. No spectral subbands are found in the range of 400-450 nm in Figure 5, which is similar to the reported spectrum of naphthalene in both solution [74] and in vapor [75]. A reported spectrum containing the weak band at 312 nm, two peaks at 320 and 335 nm, and shoulders at 348 and 360 nm [79] is very similar to our spectrum in Figure 5. Since our measurements at λ_{exc} = 280 nm coincides well with that of naphthalene in cyclohexane measured at room temperature with λ_{exc} = 270 nm using the standard 90˚

angle [79], we therefore conclude that our measurement using the angular accessory delivers the correct determination of the main vibronic transitions in the spectrum of naphthalene, without giving rise to any spectral distortions [72]. The advantages of angular excitation of fluorescence are applicable even for strongly fluorescent compounds as naphthalene, with a reported quantum yield of 0.23 when excited at 270 nm [79].

We also performed numeric fitting of the peaks in the spectrum in Figure 5 via a multi Gaussian function [80]. Figure 5B shows the numeric curve fitting and peak assignments for naphthalene. All five peaks (312 nm, 323 nm, 335 nm, 350 nm and 368 nm) were fitted with multiple Gaussian peaks, and the sixth broad curve corresponds to the spectral background. The area of each peak is indicative of the intensity of the given vibronic transition. Whereas, it is hard to exactly fit the small shoulder due to the 0-0 transition in Figure 5B, we compared the relative ratio of areas (A) of two major transitions (0-1 and 0-2), and this ratio appears to be A(0-2)/A(0-1) = 1.65. Since the spectrum is well-resolved and naphthalene is a strongly fluorescent molecule, we used naphthalene molecule as a fluorescent probe to study how the adsorption on the MOFs would affect its molecular environment. We hypothesized that the in-plane vibronic 0-1 and 0-2 transitions in naphthalene molecule are sensitive to the changes of its molecular environment. We investigated 1) pure naphthalene, 2) the solvent effect in a solid solution of eicosane, and 3) the effect of metal sites or linkers surrounding naphthalene when it is located inside the MOF cavity.

3.1.2 Fluorescence spectrum of pure naphthalene

We excited pure solid naphthalene (Figure 6) using the same settings (λ_{exc} = 280 nm, excitation and emission slits of 5 nm) that we used for the excitation of emission from naphthalene in solution (Figure 5). Also, a fluorescence spectrum with the higher resolution at λ_{exc} = 280 nm (data not shown), but with a narrower bandwidth (excitation and emission slits changed to 2.5 nm) gave a similar spectral shape.

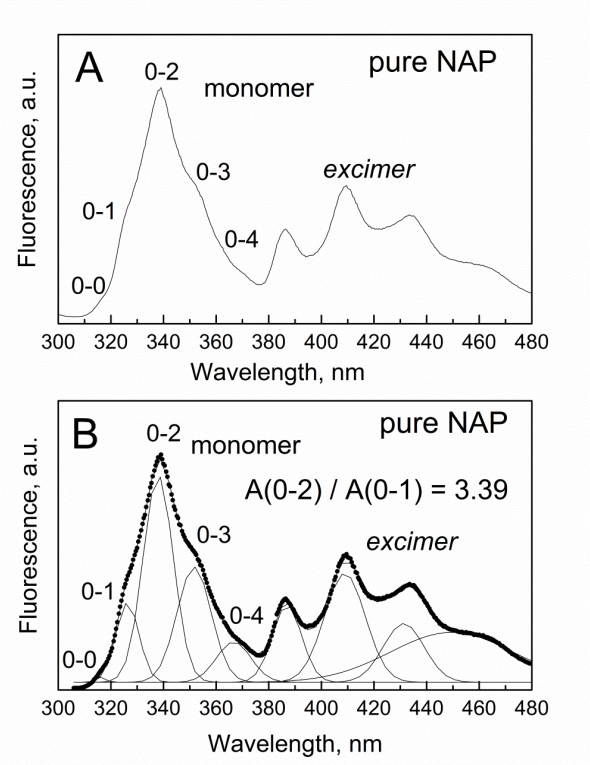

Figure 6: Fluorescence spectra of (A) pure naphthalene (NAP) at λ_{exc} = 280 nm; (B) pure NAP with its multi-Gaussian curve fitting.

As expected, the intensity of the fluorescence from pure naphthalene (Figure 6A) is much higher than that of naphthalene in dilute solution of n-heptane (Figure 5A). The emission at 310-380 nm in Figure 6A resembles that of naphthalene in dilute solution. However, the new vibronic sequence at 380-480 nm (Figure 6A) occurs, and this may be because each naphthalene molecule is now associated with other naphthalene molecules.

These new fluorescence peaks are found at 386, 409, 434 and 462 nm. In fact, the fluorescence from excimers (dimers) in pure naphthalene is well-known. Our peak at 386 nm is in agreement with the published Frank-Condon 0-0 transition for the naphthalene excimer of 3.167 eV at 391 nm [81] and 3.129 eV at 396 nm [82]. There are a few discrepancies in the assignment of spectral maxima, and these inconsistencies are likely due to red shifts caused by re-adsorption artifacts when using the standard 90˚ angle in the published reports [75,82]. The spectrum in Figure 6A also matches the fluorescence spectrum of pure naphthalene at room temperature reported earlier [71]. According to Patil *et al*. [71], the bands at 360-450 nm in the spectrum of pure naphthalene were due to the excimer fluorescence. Thus, we assign our fluorescence bands at 380-480 nm in Figure 6A to the 0-0 transition and vibronic transitions of the emission from naphthalene excimers.

The study on the molecular environment of adsorbed naphthalene molecules has been reported using the fluorescence spectrum of naphthalene excimers [83]. Specifically, within the hydrophilic inner surface of the nanopores in the cellulose sorbent, the formation of the adsorbed naphthalene excimers is favored due to hydrophobicity of naphthalene molecule [83]. Hence, we need to compare the fluorescence emission at 300-380 nm for the naphthalene monomer with the 380-480 nm for the naphthalene excimer in different samples, i.e., different molecular environments.

Specifically, looking at the spectrum for pure naphthalene there are five fluorescence peaks in the emission range of 300-380 nm (Figure 6a): at 315 nm, 325 nm, 338 nm, 354 nm, and 368 nm. The positions of these peaks are in good agreement with those obtained with 0.08 M solution of naphthalene in n-heptane (Figure 5A), and they correspond to the

emission from naphthalene monomer. In the fluorescence spectrum of pure naphthalene (Figure 6A), we assign the peak at 315 nm to the 0-0 transition, the peak at 325 nm to the 0-1 vibronic transition, the peak at 338 nm to 0-2 vibronic transition, the peak at 354 nm to 0-3 vibronic transition, and the peak at 368 nm to 0-4 vibronic transition. The assignment of the 0-0 transition is also consistent with the published 0-0 energy of $1A_1 \rightarrow 1L_b$ fluorescence transition at 315 nm in solid naphthalene [82].

Comparing the spectrum of the monomer in pure naphthalene (Figure 6A) with that of naphthalene monomer in solution (Figure 5A), we noticed that the 0-1 transition of the naphthalene monomer in pure solid naphthalene is much lower in intensity than that of the 0-2 transition. We applied numeric multi-Gaussian fitting to the spectrum of pure naphthalene (Figure 6B). The relative ratio of areas of two peaks representing two major vibronic transitions in pure naphthalene is A(0-2)/A(0-1) = 3.39. This ratio turns out to be significantly higher than the same ratio for the naphthalene monomer in solution (Figure 5B), where A(0-2)/A(0-1) = 1.65. Thus, we discovered a significant difference of the relative intensity of the 0-2 transition versus 0-1 transition in pure naphthalene. This indicates that coupling of the in-plane vibration of naphthalene at 1,380 cm^{-1} with vibronic states of the neighbor naphthalene molecule is preferred in pure naphthalene. This "coupling" effect of naphthalene molecules in pure naphthalene is in agreement with the observation of the excimer fluorescence (Figure 6A) which is absent in the spectrum of naphthalene in solution (Figure 5A). Consequently, we hypothesize that we could use the relative ratio of the areas A(0-2)/A(0-1) as an quantitative parameter to learn about the molecular environment of adsorbed naphthalene in the solid phase.

3.1.3 Fluorescence spectrum of the stoichiometric complex of F300 and naphthalene in eicosane

After the analysis of the fluorescence spectra of pure naphthalene and naphthalene molecules in solution, we proceeded with the fluorescence analysis of naphthalene molecules adsorbed on F300 MOF. First, neat solid eicosane does not have any fluorescence, as was confirmed by our reference experiments. It is also believed that only adsorption complexes of the MOFs with CUS of the d^0 or d^{10} metallic elements would emit the linker fluorescence [70]. With a Fe^{3+} electronic configuration of [Ar] $3d^5$, strong fluorescence emitted either from BTC linker or from Fe^{3+} cations in F300 MOF is not expected. In fact, pure F300 and F300 in eicosane matrix show no fluorescence emission peaks between 280 and 800 nm, as was determined by us in the reference experiments (data not shown). In order to compare the fluorescence spectrum of F300 and its complex with naphthalene, we prepared the stoichiometric complex of F300 MOF and naphthalene in a matrix of the non-fluorescent eicosane, which is solid at room temperature. According to our reference experiments, both F300 and eicosane do not exhibit detectable fluorescence emission signals under our excitation conditions, and thus this allows us to analyze the fluorescence spectrum of naphthalene in a sample containing F300 and eicosane.

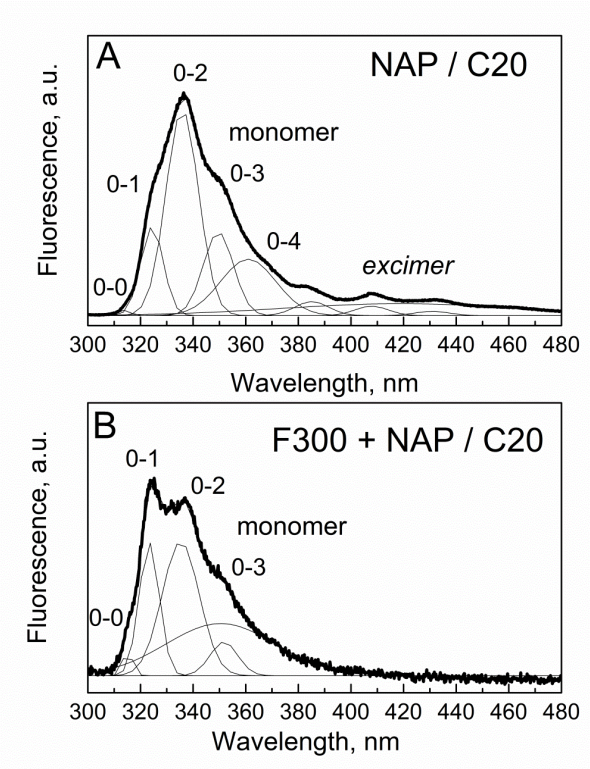

Figure 7. Fluorescence spectra of (A) 0.08 M solid solution of naphthalene (NAP) in eicosane at λexc = 280 nm and its multi-Gaussian curve fitting; (B) stoichiometric adsorption complex of F300 with NAP in 0.08 M solid eicosane and its multi-Gaussian curve fitting

To analyze the fluorescence spectra of naphthalene with and without F300 in eicosane matrix, we obtained the spectrum of naphthalene in an eicosane matrix as a blank spectrum. Figure 7A shows the fluorescence spectrum of a 0.08 M solid solution of naphthalene in eicosane photoexcited at 280 nm. The fluorescence spectrum of naphthalene in eicosane resembles that of pure naphthalene in three respects. First, the positions of the 0-0 transition and vibronic transitions of naphthalene monomer (between 300 and 380 nm) are the same as those of pure naphthalene (Figure 6A). This is predictable due to the expected weak interactions between isolated naphthalene molecules in dilute solution [84] and the nonpolar solvent molecules. Second, the relative

intensities of each vibronic transition of naphthalene monomer correspond well to those of naphthalene monomers in pure solid naphthalene. Especially, the 0-2 transition is higher in intensity compared to the 0-1 transition. Third, the low-intensity emission bands from naphthalene excimers appear at 380-460 nm, which suggests a phase separation of naphthalene from eicosane.

The phase separation of naphthalene from eicosane causes some naphthalene molecules to aggregate into clusters even in a dilute solid solution. As a result, it gives rise to a small amount of naphthalene excimers present in eicosane matrix. Again, we applied the nine-Gaussian numeric fitting to the spectrum (Figure 7A), and the relative ratio of area A(0-2)/A(0-1) is equal to 3.35, which is close to that calculated by us for the pure naphthalene (Figure 6B). On the other hand, this ratio is different from that of naphthalene in liquid solution of n-heptane, A(0-2)/A(0-1) = 1.65, Figure 5B. Therefore, given the above values of the ratio A(0-2)/A(0-1), we are able to determine the molecular environment of naphthalene in a solid eicosane matrix. Naphthalene molecules in eicosane are phase separated and thus form the excimers, while naphthalene molecules in 0.08 M liquid solution of n-heptane are isolated and exist solely as monomers.

We have obtained the fluorescence spectrum for the stoichiometric complex of naphthalene and activated F300 in eicosane matrix (Figure 7B). A significant change is noticed in comparison with the spectrum of naphthalene in eicosane (Figure 7A). That is, the spectrum of stoichiometric complex (Figure 7B) is reminiscent of naphthalene in a *liquid* 0.08 M solution in n-heptane (Figure 5A). First, the positions of all vibronic transitions are the same as those of naphthalene monomers. This means that no spectral shift took place in the spectrum of the stoichiometric adsorption complex of naphthalene

with F300 MOF in a matrix of eicosane. It is known that a red shift is likely to happen in the fluorescence spectrum when there is secondary adsorption caused by a strongly adsorption substance (F300 in this case).Since no such secondary adsorption artifact exists in our fluorescence spectra, we conclude that no significant electronic interaction between naphthalene molecules and F300 occurs.

Moreover, the 0-2 transition in the spectrum of the stoichiometric complex of naphthalene and F300 is about the same intensity as 0-1 transition, which is also noticed in the spectrum of 0.08 M naphthalene solution in n-heptane (Figure 5A). We applied the five-Gaussian numeric fitting to the spectrum (Figure 7B) and obtained the relative ratio of area A(0-2)/A(0-1) = 1.86, which is also close to the A(0-2)/A(0-1) = 1.65 for naphthalene in dilute solution of n-heptane. In addition, no emission bands at 380-460 nm from naphthalene excimers are observed in the spectrum of the stoichiometric complex of naphthalene and F300 (Figure 7B). This indicates that, although the complex of naphthalene and F300 is a solid, naphthalene molecules are well dispersed in this sample. In comparison with the spectrum of 0.08 M solid solution of naphthalene in eicosane, the molecular environment of the adsorbed naphthalene in sample with F300 is different, and it strongly affects the vibronically-coupled vibrations of adsorbed naphthalene molecules. Furthermore, we have measured the fluorescence spectrum of a 0.08 M solid solution of naphthalene in eicosane (Figure S3A) and the stoichiometric complex of naphthalene with F300 in eicosane (Figure S3B) at λ_{exc} = 300 nm. For this data, numeric fitting was not effective due to large overlapped area of Raleigh peak at 300 nm and emission spectrum of naphthalene at 310-460 nm. Qualitatively, however, the same conclusions are obtained as for λ_{exc} = 280 nm (Figure 7).

After a detailed analysis of the fluorescence of naphthalene in various molecular environments using naphthalene as a "self-probe", we have two major observations about the stoichiometric complex of naphthalene and F300: 1) the absence of excimer emission and 2) 0-2 transition with a comparable intensity to that of 0-1 transition. We explain these effects as a consequence of confinement of naphthalene molecules adsorbed in the mesoporous cavity of F300. Confinement of aromatic molecules in the nanopores of the sorbent was observed via the change of relative intensity of emission bands from monomers and excimers [83]. This is to say, naphthalene molecules exist as monomers when adsorbed in the cavity of F300, like those in the liquid solution of n-heptane. These findings also suggest a hydrophobic environment in the cavity of F300 MOF that is a part of the adsorption complex with naphthalene, due to the surrounding non-polar BTC linkers. Essentially, the cavity size (21 Å) of F300 is definitely large enough to trap naphthalene molecule with kinetic diameter of 6.57 Å. To further study this phenomenon, as well as the orientation of naphthalene in the adsorption complex, we conducted our experiments using near-UV/Vis DRS to study the electronic interactions of indole in an adsorption complex with F300.

3.1.4 Near-UV/Vis DRS of adsorption complexes of F300 with naphthalene or indole

The traditional way of measuring the near-UV/Vis DRS spectrum is to mix the solid sample with $BaSO_4$ powder and to use $BaSO_4$ powder as a spectroscopic reference. However, in our case, our MOFs are highly sensitive to the moisture or oxygen in air. Thus, we conducted the near-UV/Vis DRS measurements in a closed quartz fluorescence cuvette to protect our sample from ambient air. Likewise, the near-UV/Vis DRS spectrum of adsorption complex of HKUST-1 was measured in a closed quartz vessel [7]. It was

suggested by Mössbauer spectroscopy [14] that in both as-prepared and activated F300, iron exists as Fe^{3+}. The adsorption of light by Fe^{3+} yields a light-brown color of the sample, and the color did not change when the adsorption of naphthalene on F300 took place.

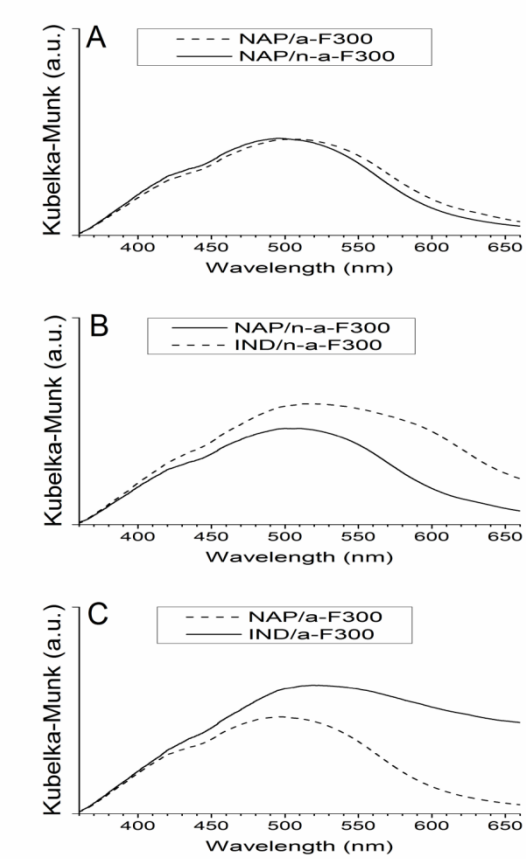

Figure 8. The near UV/Vis DRS of (A) NAP with non-activated F300 *vs*. NAP with activated F300; (B) NAP with non-activated F300 *vs*. IND with non-activated F300; (C) NAP with activated F300 *vs*. IND with activated F300.

Based on our previous findings, naphthalene has rather weak interactions with F300. Therefore, we increased the amount of naphthalene molecules in the sample with F300 to promote the formation of the adsorption complex of naphthalene with F300. As shown in Figure 8A, we compared the near-UV/Vis DRS spectrum of the solid mixture of excessive naphthalene and non-activated F300 (n-a-F300) with that of the mixture of

excessive naphthalene with activated F300 (a-F300). The molar ratio of naphthalene versus F300 is n(NAP)/n(F300) = 50 for both samples. The near-UV/Vis DRS spectrum in Figure 8A shows no observable difference between two samples despite there being, potentially, two distinct coordination environments, specifically, Fe^{3+} with coordinated water (in the n-a-F300) and Fe^{3+} CUS (in the a-F300). The Fe^{3+} cations in the non-activated F300 are coordinated with adsorbed water, oxygen or excess of BTC, while there are CUS available in the activated F300. Since naphthalene has no adsorption bands [74] in the range shown in Figure 8, we observed no spectroscopic evidence of the formation of coordination bonds by Fe^{3+} and naphthalene in either activated or non-activated F300 (Figure 8A). In other words, the near UV/Vis DRS spectra do not support the presence of either coordination or the π-π interactions between adsorbed naphthalene molecules and the CUS or aromatic linkers in F300 MOF. Apparently, the bonds in the adsorption complex of naphthalene with F300 MOF are weak, and rather advanced spectroscopic methods are needed to detect them, supported by quantum chemical computations.

Next, we prepared mixtures containing molar excess of indole with non-activated F300 and activated F300. The molar-ratio of indole (IND) molecules versus F300 is n(IND)/n(F300) = 50 for both samples. When mixing with naphthalene, the light-brown color of F300 became significantly darker. The mixture of indole and non-activated F300 has a “chocolate” color, and the mixture of indole and activated F300 has an even darker color. The near-UV/Vis spectra of the mixtures of indole with F300 and mixtures of naphthalene with the n-a-F300 are presented in Figure 8B. Indole has no adsorption band in the spectral range shown, and thus, the spectrum is indicative of some electronic

interaction taking place between the iron cluster of F300 and indole adsorbate. In comparison with the mixture of naphthalene with non-activated F300, there is a significant enhancement in optical absorbance at 460-660 nm, which indicates a change in coordination environment of Fe^{3+} in the non-activated F300 upon adsorption of indole. Furthermore, this statement is strengthened by the near-UV/Vis DRS spectrum of the mixture of indole with activated F300 (Figure 8C).

In comparison with the spectrum of mixture of naphthalene with activated F300, the adsorption band at 460-660 nm in spectrum of mixture of indole with activated F300 is apparently higher due to interactions of Fe in F300 MOF with indole upon adsorption. In fact, the band in the spectrum of the mixture of indole with activated F300 is even higher than that of the mixture of indole with non-activated F300 (Figure 8B), and it is very likely due to a larger amount of CUS available in the activated F300 than in non-activated F300. Hence, we conclude that the adsorption bands at 460-660 nm in the spectra of the mixture of indole with activated *vs*. non-activated F300 demonstrate the electronic interactions between adsorbed indole molecule and the Fe^{3+} CUS in F300 MOF, specifically, the coordination bonds. Here, we report a direct spectroscopic proof of the coordination bonds between metal sites in the MOF and N-heterocyclic "guest molecules" by near-UV/Vis DRS for the first time. Further study is needed to have a more detailed understanding of this electronic interaction.

3.1.5 Fluorescence spectra of the mixtures of indole and F300

We performed a fluorescence spectroscopy study of the adsorption complexes of indole with activated F300 or non-activated F300. In order to obtain the fluorescence spectrum of the mixtures of indole and F300, we intentionally add an excessive indole

amount (*vs*. the anticipated stoichiometric amount) to the sample containing F300 MOF. Both F300 MOF and indole have rather weak fluorescence, thus their adsorption complex would likely exhibit fluorescence with a distinct spectral position and shape. First, we obtained a fluorescence spectrum of pure indole using the angular fluorescence accessory (Figure 9A). It is reported that the room temperature fluorescence spectrum of indole starts at around 280 nm [85]. Thus, we photoexcited indole at 260 nm to get a full spectrum. We prepared the mixtures of indole with F300 with two different molar ratios, R_1 = n(IND)/n(F300) = 50 (Figure 9B) and R_2 = n(IND)/n(F300) = 15 (Figure 9C).

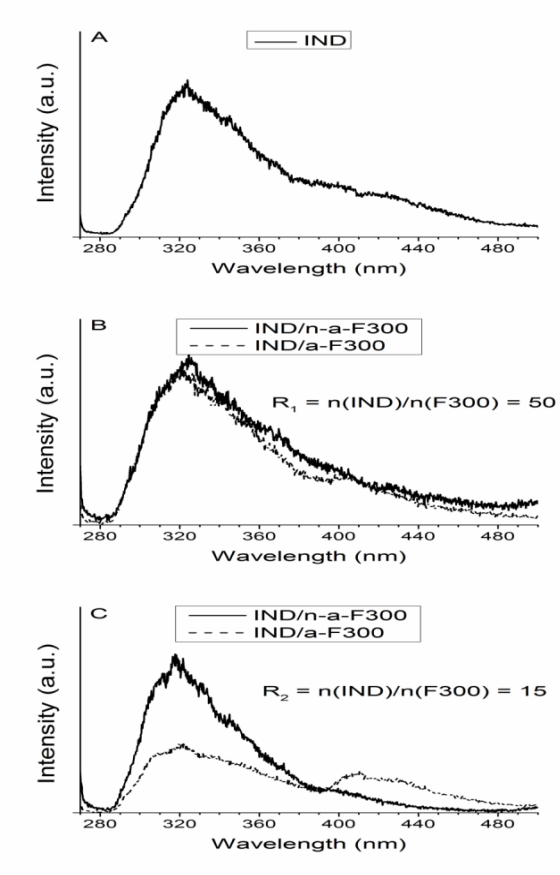

Figure 9: Fluorescence spectra of (A) pure IND at λ_{exc}=260 nm; (B) IND with n-a-F300 and IND with a-F300 at λ_{exc}=260 nm, R_1=50; (C) IND with n-a-F300 and IND with a-F300 at λ_{exc}=260 nm, R_2=15.

From the spectrum of pure indole (Figure 9A), we observed an emission peak at 320 nm and a broad band at 380-480 nm following the peak. The emission peak at 290-380 nm with a weakly resolved structure was assigned to indole monomer emission, consistent with emission of indole in solution by the previous study [86]. Thus, we assign the emission peak at 290-380 nm (Figure 9A) to the emission from indole monomer in our sample. Based on our previous study on the fluorescence of naphthalene excimers (Figure 6), we suggest that the emission band at 380-480 nm (Figure 9A) should be assigned to the emission from indole excimers due the similar molecular weight molecular structure, and adsorption spectra between indole and naphthalene. The emission band from indole excimers has a weakly resolved vibronic structure, similar to the emission from indole monomers.

Next, we performed the fluorescence measurement of the mixture of indole with activated and non-activated F300 at R_1 = n(IND)/n(F300) = 50 (Figure 8B). For both samples, the emission bands from indole monomers resemble those from indole monomers in pure indole. However, the weakly resolved vibronic structure of indole excimers at 380-480 nm is missing in the spectra of both mixtures of indole with activated and non-activated F300. This might indicate the inhibition of the formation of indole excimers when F300 MOF is present. Yet, by comparing the spectrum of the mixture of indole and non-activated F300 with that of the mixture of indole and activated F300, we observed a new emission peak at 410 nm only in the spectrum of the mixture of indole with activated F300, while the broad band from indole excimers at 410 nm slightly declines. Thus, the origin of the peak at 410 nm (Figure 9B) is distinct from that of the broad emission band from indole excimers in pure indole (Figure 9A). In addition, the

new emission peak only exists in the spectrum of the mixture of indole with activated F300, but not in that of the mixture of indole with non-activated F300. This can be explained by a lack of available Fe^{3+} CUS in the non-activated F300. Hence, we hypothesized that the emission peak with a maximum at 410 nm (Figure 9B) has its origin in the adsorption complex formed by indole and Fe^{3+} CUS in activated F300. We propose the formation of the adsorption complex as follows:

F300 + IND → Complex.

If our assumption (that the formation of adsorption complex gives rise to a new fluorescence peak at 410 nm even in a nonstoichiometric mixture with a large molar excess of indole *vs*. F300 MOF) is correct, then a smaller molar excess of indole molecules in mixtures would give a clearer emission at 410 nm with less interference from indole emission. To prove this hypothesis, we measured the fluorescence spectra of the mixtures of indole with activated and non-activated F300 at R_2 = n(IND)/n(F300) = 15. While preparing the mixtures, we tried to maintain the sample in same solid phase at room temperature, and the ratio R_2 = n(IND)/n(F300) = 15 is the lowest molar ratio for the sample we could prepare. The fluorescence spectra of the mixtures of indole with activated and non-activated F300 are shown in Figure 9C. Again, a change in the relative intensities of two highest transitions in emission bands of indole monomer is observed. In the mixtures of indole with activated or non-activated F300, the shoulder at 310 nm is just slightly lower than that at 325 nm, while in pure indole the intensity of shoulder at 310 nm is much lower that at 325 nm. Although the weakly resolved vibronic structure does not allow the numeric fitting for the spectra of indole or the mixtures of F300 with indole, a similar behavior was observed and discussed for pure naphthalene versus

naphthalene with F300 (Figure 6 & Figure 7B). Hence, the confinement of adsorbed indole in the mesocavity of F300 MOF is suggested. Furthermore, by comparing Figure 9B and Figure 9C, the emission peak at 410 nm in the spectrum of mixture of indole with activated F300 at R_2 = n(IND)/n(F300) = 15 is even higher than that of the mixture of indole with activated F300 at R_1 = n(IND)/n(F300) = 50 as expected. This is to say, a higher amount of activated F300 mixed with an excessive indole (to promote the formation of relatively weak adsorption complex) gives a stronger emission at 410 nm, which is hypothesized to originate from the adsorption complex. Thus, the peak at 410 nm has emission of photons from the excited state of indole that contributes to the molecular orbitals forming the excited electronic state of the adsorption complex of indole with F300. Finally, since the emission peak at 410 nm is only present in the spectra of the mixtures of indole with activated F300 which has available Fe^{3+} CUS, we therefore conclude that the fluorescence peak at 410 nm is due to the electronic interaction between indole and Fe^{3+} CUS in the activated F300.

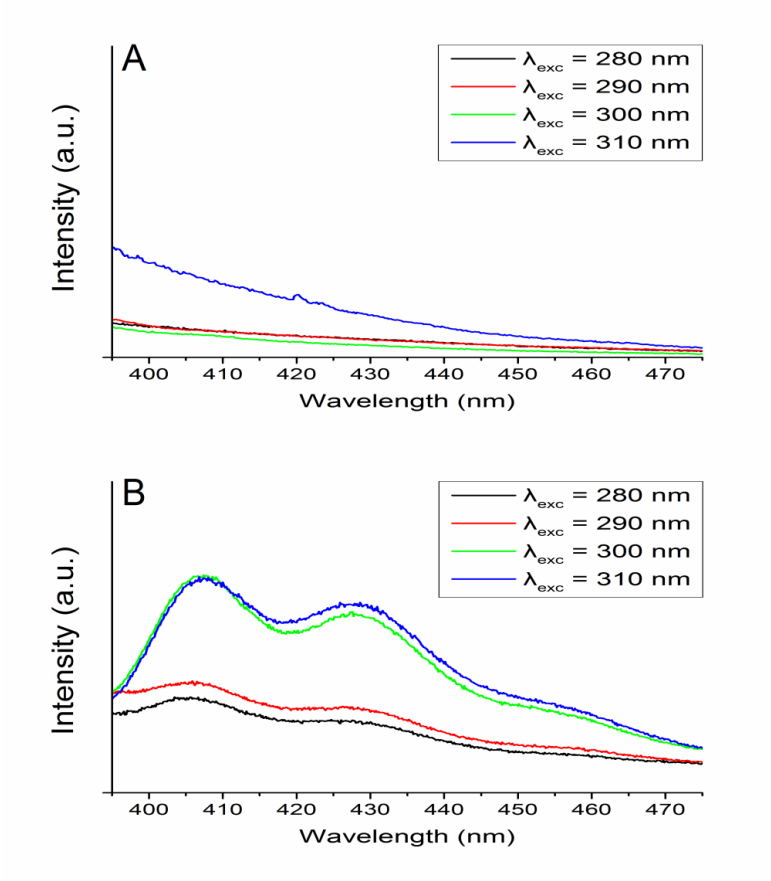

Figure 10. Fluorescence spectra of (A) pure IND at λ_{exc}= 280, 290, 300 and 310 nm; (B) IND with a-F300 at λ_{exc} = 280, 290, 300 and 310 nm at R_2=15.

Due to the fact that the fluorescence from the adsorption complex at 410 nm is close to the fluorescence from pure indole at 380-480 nm, we need to further investigate these two emission bands in order to clearly distinguish between them. In Figure 10A, we show the wavelength-dependent fluorescence spectra of pure indole at various excitation wavelengths. As expected, there are no fluorescence peaks in the spectral range of interest. On the other hand, in Figure 10B, the well-resolved fluorescence at different λ_{exc} (280, 290, 300 and 310 nm) for the mixture of indole with activated F300 at R_2 = n(IND)/n(F300) = 15 has revealed two distinct peaks at 407 nm and 430 nm. Considering that the wavelength-dependent fluorescence of pure indole does not give any peaks at the

designated area where the fluorescence peaks from the adsorption complex is observed, the fluorescence emission from the adsorption complex is distinguished from that of indole. Furthermore, the intensity of the fluorescence of the adsorption complex is dependent on the excitation wavelength (Figure 10B).

According to the UV/Vis DRS spectrum of the mixture of indole with activated F300 (Figure 8), there are enhanced adsorption bands at 460-660 nm due to coordination of indole onto Fe^{3+} CUS in F300. We have collected the fluorescence spectra at excitation wavelength 468 and 605 nm to check whether the photoexcitation of those electronic transitions in the visible range would cause any fluorescence in the visible and near-IR range. However, no fluorescence was observed. Thus, there are two distinct types of electronic transitions present in the adsorption complex of indole with activated F300. First, these are absorbance bands at 460-660 nm which originate from the coordination bond between indole and Fe^{3+} CUS in F300 and that cause no fluorescence emission. On the other hand, we found the optical absorbance of the adsorption complex at excitation wavelengths between 280 and 310 nm causes the emission of distinct structured fluorescence at 395-475 nm (Figure 10B). Therefore, the wavelength-dependent fluorescence spectroscopy in the solid state with angular accessory can detect the distinct fluorescence emissions from the adsorption complex even in the presence of molar excess of indole in the mixture with activated F300. Further work is needed to determine the origin of any fluorescence from the adsorption complexes of substituted indoles and F300 in near UV and visible ranges.

3.1.6 Kinetics of the formation of adsorption complex of indole with activated F300

Having detected the distinct fluorescence emission bands from the adsorption complex of indole with activated F300, we proceeded to study the kinetics of the formation of this adsorption complex using time-dependent fluorescence spectroscopy. We set the sample temperature at 60 ˚C and the excitation wavelength at 310 nm, which is optimal for the excitation of the adsorption complex, with continuous stirring of the suspension under argon. Figure 11 shows the fluorescence spectra of the adsorption complex of indole with activated F300 present as powder suspended in liquid indole. Each progressive scan of the spectrum took 6.6 minutes, and the scans #1, 4, 7, 10 and 13 are shown in Figure 11A, while the scans #16, 19, 22, 25 and 28 are shown in Figure 11B.

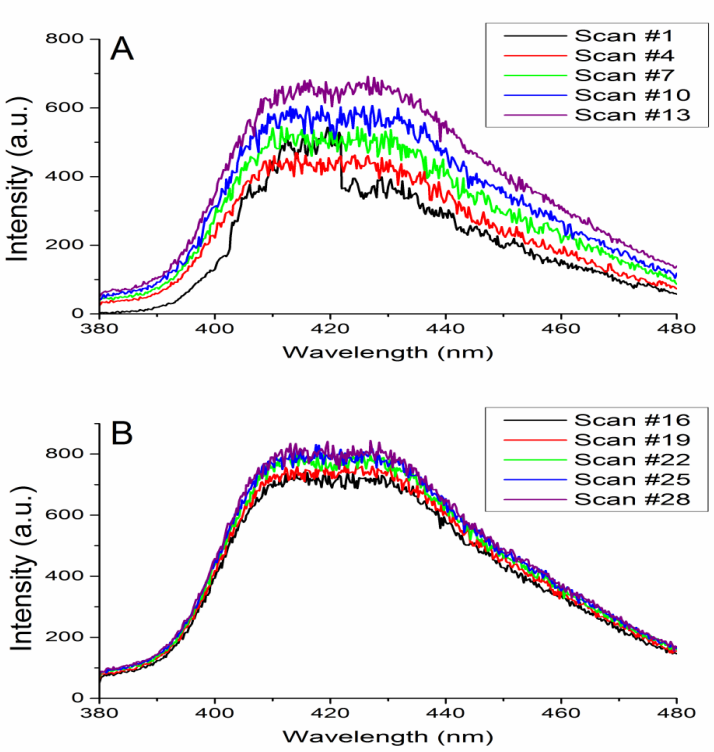

Figure 11. The time-dependent fluorescence spectra of the adsorption complex of a-F300 and indole in liquid indole, at λ_{exc} = 310 nm, 60 ˚C, and 6.6 min per scan. (A) Scans #1, 4, 7, 10, 13. (B) Scans #16, 19, 22, 25, 28.

First, we observed the emission bands with peaks at 407 and 430 nm from the adsorption complex in Figure 11A, with steadily increasing fluorescence intensity as adsorption was proceeding. The first two fluorescence spectra obtained are different from the rest, and this difference is due to incomplete melting of the solid mixture of indole and activated F300 at the beginning of the continuous scans (see Experimental). After the first two spectra, all subsequent spectra maintained the same shape with emission bands at 380-480 nm. The intensity kept increasing for about 12 scans (approximately 80 minutes), after that the intensity of those emission bands (scans #16 through #28 in Figure 11B) increased at a much slower speed than before (Figure 11A). After the scan #28 (approximately 180 minutes total adsorption time), the fluorescence spectra did not increase. Thus, the equilibrium of the adsorption process was reached.

We used our assumption of the formation of the adsorption complex to build the kinetic model of adsorption of indole onto activated F300 in liquid phase. The formation of the adsorption complex is: F300(solid) + IND(liquid) → Complex(solid). First, no fluorescence is detected for the reactant F300, and thus no information is available about the kinetic order of the adsorption of indole on F300 by reactant. Second, indole as a reactant also serves as the solvent, which means that the concentration of indole is constant. Therefore, the influence of the concentration of reactant indole on the rate of the kinetics of adsorption cannot be determined. Third, the product of adsorption (the adsorption complex) is present as minority component at an early stage of adsorption (during the scans #1-10 in Figure 11A). Hence, the concentration of the adsorption complex can be analyzed by chemical kinetics formalism, under the assumption that at a low concentration of the adsorption complex at early stage of adsorption and without re-

absorption of light and scattering effects [72], the intensity of the fluorescence is proportional to the concentration of the adsorption complex in the suspension.

Next, we attempted to analyze the dependence of the integrated area in the fluorescence spectra on the adsorption time at constant temperature (60 ˚C). The dependence of the assumed concentration as function of adsorption time corresponds to the integrated kinetic zeroths order rate law of adsorption. At the early stage of adsorption (before 80 minutes), the integrated area of the fluorescence spectra was fitted with linear dependence, and resulted in a time constant k equal to 189.3 ± 2.8 min^{-1}. The coefficient of determination R^2 (correlation coefficient) is 0.998, and the error of determination is 1.5%. At the later stage of adsorption, the dependence is not linear, and the integrated area of the fluorescence spectrum reaches a plateau. The zeroth-order kinetics of adsorption found by us is consistent with the reported zeroth-order kinetic rate law of heterogeneous photocatalysis in the "liquid-solid" system where the adsorption is a rate-limited process [87], and with the kinetics of desorption of the small-molecule drugs via hydrolysis of adsorption complexes formed with MIL-100 and MIL-101 MOFs [26]. Apparently, the kinetics of adsorption of indole on F300 MOF is diffusion-limited, and this is consistent with the highly porous structure of the F300 sorbent.

3.1.7 Fluorescence spectra of the "pure" adsorption complexes of F300 and MIL-100(Fe) MOFs with indole and naphthalene

After the studies of the fluorescence of adsorption complex of indole and F300 MOF in the presence of a molar excess of indole, we decided to investigate the fluorescence of adsorption complexes of activated F300 with indole. These complexes were obtained after evaporation of volatile solvent n-heptane and any weakly bound substances

including non-adsorbed indole (see Experimental section). It is well-known that the MOFs have large pore cavities and inherently low bulk density. Therefore, it is hard to prepare the uniform solid solution with indole at stoichiometric molar ratio with F300 by mixing pure indole with F300 directly. Furthermore, the efficiency of adsorption cannot be measured by this method. Instead of making the stoichiometric complex by mixing pure indole with activated F300 directly, we allowed the activated F300 to react with solution of indole at room temperature, and evaporated the obtained suspension (presumably containing the adsorption complex suspended) in n-heptane to make the "pure" adsorption complex. Upon adsorption of indole from solution onto F300, the color of F300 changed from a light brown to dark brown, and this transformation is reminiscent of the color change of the solid mixture of indole and activated F300 (Experimental section 2.7). We have obtained the fluorescence spectra both before and after evaporation. Figure 12A shows the spectrum of the suspension of the complex of indole with activated F300 in n-heptane. Figure 12B shows the spectrum of the complex of indole with activated F300 after evaporation under high vacuum ($<1 \times 10^{-3}$ Torr). Figure 12C shows the spectrum of activated F300.

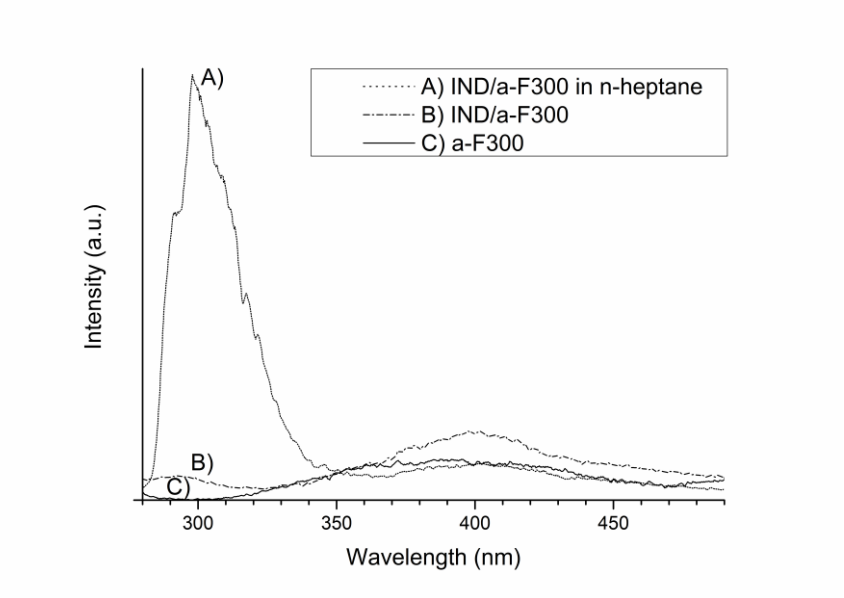

Figure 12. Fluorescence spectra of A) adsorption complex of a-F300 with indole in n-heptane at λ_{exc} = 260 nm; B) adsorption complex of a-F300 with indole; C) a-F300 at λ_{exc} = 260 nm.

First, we obtained the fluorescence spectrum of activated F300 (Figure 12C), we see a broad emission band with low intensity at 310-480 nm. Next, in the fluorescence spectrum of the suspension (Figure 12A), we see the fluorescence peak at 280-360 nm which resembles the fluorescence spectrum of indole monomer (Figure 9A). A blue-shift of the emission peak of the indole monomer in n-heptane from the fluorescence of indole monomer in neat indole (Figure 9A) could be explained by the change from polar environment (neighboring indole molecules in neat indole) to non-polar solvent (n-heptane solvent) [88]. Again, a broad emission at 360-480 nm is noticed, and it resembles that of activated F300. The familiar fluorescence peaks such as those in Figure 9, 10 and 11 for the adsorption complex of indole with activated F300 are, however, not observed. Thus, the expected formation of the adsorption complex of activated F300 MOF with indole is not detected.

As shown in Figure 12B, we observed the strong decrease of emission peaks at 280-360 nm, which were assigned to indole monomer (Figure 12A), after evaporation under the high vacuum ($<1 \times 10^{-3}$ Torr). This means that the majority of indole (with a total amount of indole added that corresponds to the adsorption complex, see Experimental) was not strongly bound to the adsorption sites in F300 after adsorption at room temperature in solution, and it was easily removed under the high vacuum. Instead, the spectrum of the presumed "pure" adsorption complex of indole with activated F300 (Figure 12B) is similar to the spectrum of activated F300 (Figure 12C), except for a small peak at 290 nm. The position of this peak is consistent with the spectrum of indole monomers in diluted solution (Figure 9). Therefore, we conclude that the adsorbed indole in the complex with F300 MOF is in its monomeric form. However, we were not able to detect the typical spectral bands of the adsorption complex of indole with activated F300, since bonding in the complex of indole with activated F300 is weak, and the complex is apparently non-stoichiometric, when formed from indole suspended in n-heptane.

Similarly, the competitive adsorption of indole and naphthalene onto activated MIL-100(Fe), a-MIL-100(Fe) was studied using fluorescence spectroscopy. To prepare the sample, the stoichiometric amount of activated MIL-100(Fe) was mixed with a binary solution of naphthalene (0.08 M) and indole (0.08 M) in n-heptane, and adsorption was allowed to proceed for 1 hour under continuous shaking. Since MIL-100(Fe) is known to have a similar structure to the commercially available F300, it is reasonable to expect the formation of the adsorption complex between indole and activated MIL-100(Fe). Further, due to the fact that MIL-100(Fe) possesses a similar structure to F300, it is reasonable to believe the spectrum for MIL-100(Fe) would be the similar to that of F300. Moreover,

indole is expected to interact preferably with MIL-100(Fe) due to the available Fe^{3+} in activated MIL-100(Fe), even in the presence of naphthalene in solution. Figure 13A shows the fluorescence spectrum of the complex of activated MIL-100(Fe) formed with indole and naphthalene present as equimolar binary solution in n-heptane. The spectra of the complex of activated MIL-100(Fe) with indole and naphthalene were obtained after evaporation of any non-bound volatile organic compounds in the high vacuum as in Figure 13B.

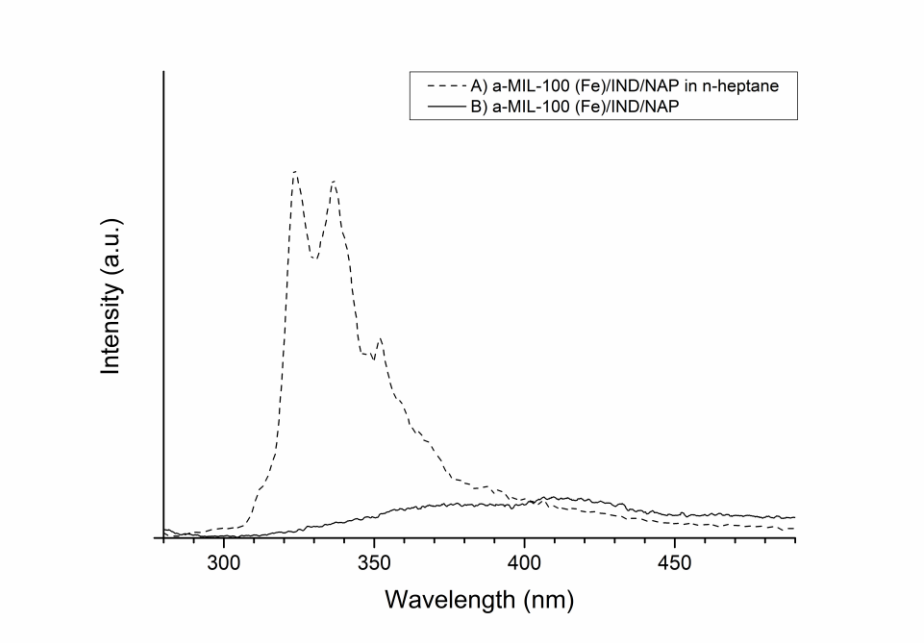

Figure 13. The fluorescence spectra of A) the suspension of the complex of a-MIL-100(Fe) with indole and naphthalene in n-heptane at λ_{exc} = 260 nm; B) the "pure" complex of a-MIL-100(Fe) with indole and naphthalene at λ_{exc} = 260 nm.

In Figure 13A, the fluorescence from naphthalene monomer in the suspension with MIL-100(Fe) is observed at 300-400 nm, and this fluorescence is much higher than the fluorescence from MIL-100(Fe) and from indole. In the "pure" adsorption complex formed from the binary solution of indole and the competing adsorbate naphthalene,

indole is not present as monomer since we were not able to detect the fluorescence of indole at ca. 300 nm.

The fluorescence from MIL-100(Fe) at 400-480 nm remains as expected. Therefore, there are no strong electronic interactions between MIL-100(Fe) and either adsorbate. The high intensity fluorescence from naphthalene monomer in suspension has disappeared completely after the evaporation in the high vacuum ($<1 \times 10^{-3}$ Torr). Moreover, the new shoulder at 350-400 nm has appeared. The origin of this new shoulder at 350-400 nm is assigned, tentatively, to the presence of both indole and naphthalene in the sample that form the stoichiometric 1:1 exciplex of naphthalene and indole [89]. This exciplex would be weakly bound to MIL-100(Fe), i.e. the naphthalene and indole would be bound more strongly to each other than to the adsorption sites in MIL-100(Fe). Thus we conclude that the adsorption complexes of activated F300 or MIL-100(Fe) with indole are not detected by the fluorescence spectroscopy, and the future studies are needed.

3.1.8 The near-UV/Vis DRS of the "pure" stoichiometric adsorption complexes of F300 and MIL-100(Fe) with indole

To further investigate the formation of the "pure" adsorption complexes with rather weak bonding, we performed near-UV/Vis DRS analysis of the adsorption complex of activated F300 *vs*. activated MIL-100(Fe) with indole. The "pure" adsorption complex of activated F300 with indole was prepared with a stoichiometric molar ratio, and the same molar ratio was used to prepare the "pure" adsorption complex of the activated MIL-100(Fe) with indole, at R = n(MIL100)/n(IND) = n(F300)/n(IND) = 1. After evaporating the suspension of the adsorption complexes in n-heptane, the dry solid adsorption complexes were obtained. Both adsorption complexes of F300 and MIL-100(Fe) with

indole have a brown color, as we observed for the solid non-stoichiometric mixtures of F300 with indole (Chapter 3.1.4). Similarly, the near-UV/Vis DRS spectra were collected from the powdered sample in a closed quartz cuvette, with protection against the ambient air. Figure 14A shows the comparison of the activated F300 *vs*. the adsorption complex of activated F300 with indole. Figure 14B shows the comparison of activated MIL-100(Fe) *vs*. the adsorption complex of activated MIL-100(Fe) with indole.

In Figure 14A, we can see the contributions from the "free" Fe^{3+} CUS in activated F300 and Fe^{3+} CUS in the adsorption complex of activated F300 with indole, and a significant absorbance enhancement in the range 360-660 nm was observed in the spectrum of adsorption complex of activated F300 with indole. However, the absorption spectrum of the adsorption complex has the same sequence of peaks as the spectrum of neat F300, although at the higher absorbance. Therefore, no new electronic transitions are formed in the adsorption complex of activated F300 MOF with indole. This is in contrast to the near-UV-Vis DRS spectra of the non-stoichiometric solid mixtures of F300 with molar excess of indole (Figure 8), where the new peaks were found due to the electronic transitions of the complex, and the minima in the spectrum of neat F300 MOF changed to the maxima in the spectrum of the complex.

Therefore, our near-UV/Vis DRS spectra of the "pure" adsorption complex of F300 and indole prepared at the 1:1 stoichiometric ratio are consistent with the fluorescence spectrum of the same complex, Figure 12, and no spectral proof of the new electronic interactions in the presumed "pure" stoichiometric complex is obtained. Therefore, this adsorption complex is weak, and it can be prepared in sufficient amounts to be detected spectroscopically only when the excess of indole adsorbate (the ligand) is present.

Similarly, an enhancement of optical absorbance in the range 360-660 nm was found in the spectrum of adsorption complex of activated MIL-100(Fe) with indole (Figure 14B). Therefore, the coordination bonds between indole adsorbate and Fe^{3+} CUS in the adsorption complex with activated MIL-100(Fe) are weak as well.

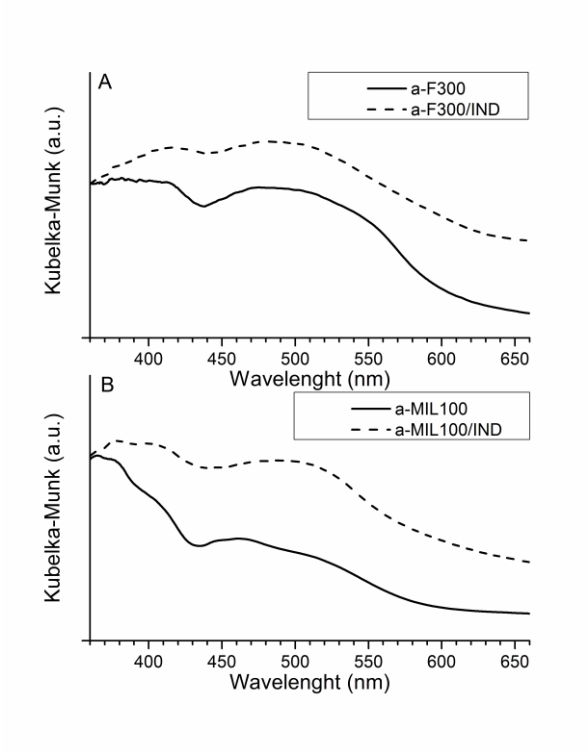

Figure 14. The near UV/Vis DRS of (A) activated F300 *vs*. IND with activated F300; (B) activated MIL-100(Fe) *vs*. IND with activated MIL-100(Fe).

3.2 The studies of adsorption of naphthalene and indole on the microporous A100 (Al) without CUS

3.2.1 The study of the origin of fluorescence in A100

The A100 MOF, which is also known as a commercially available product equivalent to MIL-53(Al), consists of Al^{3+} clusters and the dianionic form of 1,4-benzenedicarboxylic acids (BDC). Before we measured and interpreted the spectra of the

A100 MOF, we decided to determine the electronic levels that would originate from the BDC linker in A100 MOF.

We first obtained the adsorption spectrum of dianionic form of BDC in solution. The sample was prepared as 0.2 M solution of BDC in the buffer solution with pH 8.5, and then the solution was diluted 300-fold to measure its absorption spectrum. For the non-dissociated 1,4-benzenedicarboxylic acid $BDCH_2$, the pKa1 = 3.41 and pKa2 = 4.82 [90]. Therefore, at pH=8.5 (Figure 15), both carboxylic groups of $BDCH_2$ are dissociated to form the dianionic form $(BDC)^{2-}$. This means that in this solution, the BDC is present in the same completely deprotonated form as it is present in A100 MOF, and this solution is a good model system to study the energy levels in the A100 MOF.

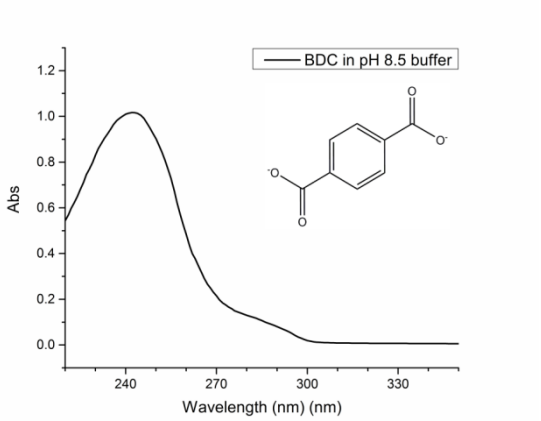

Figure 15. The UV/Vis absorption spectrum of 1,4-benzenedicarboxylic acid in dianionic form in the buffer solution with pH 8.5.

As shown in Figure 15, two broad adsorption peaks are present in absorption spectrum, respectively at 242 and 286 nm. Thus, we proposed the energy level diagram including S0, S1, and S2 electronic levels. The absorption at 240 nm would be due to the S0 → S2 transition, while the absorption at 290 nm would be due to the S0 → S1

transition that is also the HOMO-LUMO transition. In order to test this model, we obtained the complementary fluorescence spectra from BDC and A100 MOF.

Figure 16 shows the fluorescence spectra of 0.0007 M BDC in 0.1 M HCl, the 0.002 M solution of BDC in a buffer solution with pH 8.5, and from neat solid $BDCH_2$, and activated A100. We have observed significant similarity between the fluorescence spectrum of 1) a diluted solution of BDC in an acidic environment ($BDCH_2$), 2) the completely deprotonated form of BDC (BDC^{2-}), 3) neat solid BDC in acidic form ($BDCH_2$) and 4) A100 with formula Al(OH)[BDC].

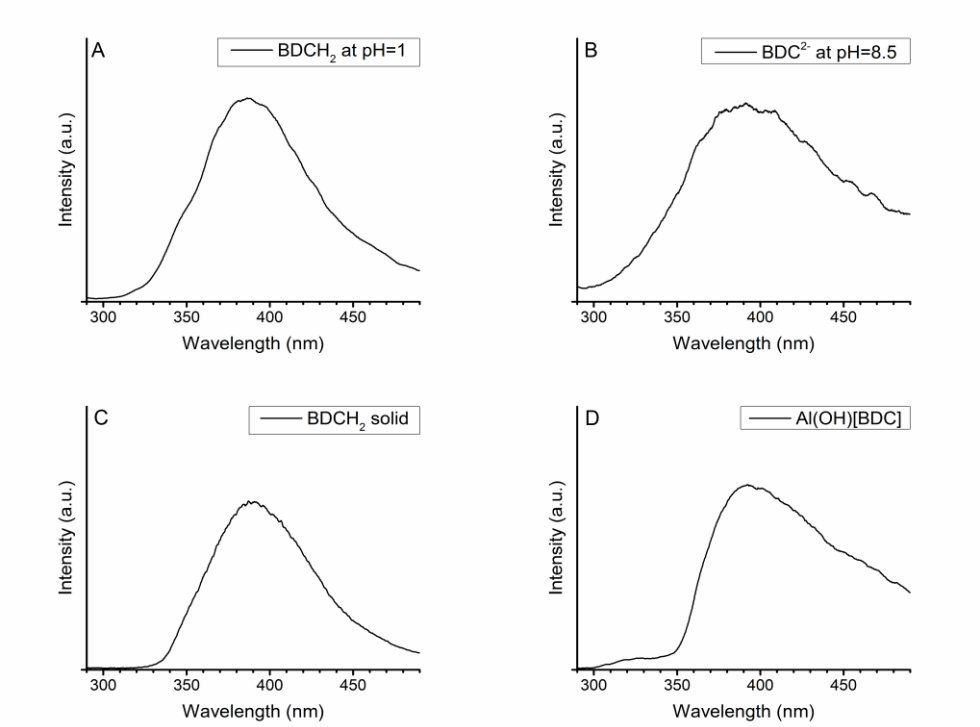

Figure 16. The fluorescence spectra at λ_{exc} = 260 nm of a) BDC in 0.1 M HCl, exc. slit 20 nm/emiss. slit 5 nm; b) BDC in pH 8.5 buffer, exc. slit 20 nm/emiss. slit 5 nm; c) solid BDC, exc. slit 20 nm/emiss. slit 5 nm; d) activated A100, exc. slit 5 nm/emiss. slit 5 nm.

The major emission peak of A100 MOF at 400 nm is consistent with the fluorescence due to the S1 → S0 transition. By comparing the spectra in Figure 16C and 16D, the

fluorescence of BDC has an emission band with maximum at 390 nm which is very similar to that of A100. It is important to note that the 0.0007 M solution of BDC in 0.1 M HCl yields the same shape of the fluorescence spectrum as the neat solid BDC and A100 MOF. This means that the fluorescence from A100 and neat BDC originates from the monomers of BDC, and not from molecular associates of BDC units in A100 MOF or the emission of associated, e.g. hydrogen bonded $BDCH_2$ molecules in neat BDC. Therefore, we hypothesized that the fluorescence of A100 is the ligand-based fluorescence originating in the monomer unit of BDC.

Specifically, based on the UV/Vis adsorption spectrum in solution (Figure 15), the fluorescence spectra of $BDCH_2$ (Figure 16A) *vs*. BDC^{2-} (Figure 16B) in dilute solution, and the fluorescence spectrum of solid $BDCH_2$ (Figure 16C) *vs*. activated A100 Al(OH)[BDC] (Figure 16D), we have obtained two conclusions. First, the similar spectral shape of BDC in acidic form (Figure 16A) and completely deprotonated form (Figure 16B) indicates the independence of the fluorescence of BDC on whether the carboxylic group is deprotonated or not. Thus, the fluorescence of BDC has its origin in the emission from the aromatic benzene ring, but not in carboxylic acid. Second, the emission at 320 nm in A100 (Figure 16D) is due to the electronic transition S2 → S0. The existence of the S0 → S2 transition is shown by experiments and DFT calculations of 2-aminoterephthalic acid with similar structure [91] to $BDCH_2$. The fluorescence at ca. 320 nm assigned to the S2 → S0 transition is a low intensity transition due to the competing de-excitation process: an effective internal conversion from S2 to S1 level, and the following high intensity emission from S1 to S0 level at 400 nm (LUMO to HOMO transition). The relative intensities of the S2 → S0 and S1 → S0 transitions in activated

A100 MOF are consistent with the well-known Kasha's rule [92]. Moreover, the fluorescence of BDC in its acidic or fully dissociated form and when it is embedded in A100 MOF has its origin in the emission from molecular orbitals formed by the π-system of phenyl group. The alternative would be to assign this emission to the $\pi^* \rightarrow n$ transition with non-bonding orbital being due to the lone electron pair on oxygen atom. However, the $\pi^* \rightarrow n$ transition involving atomic orbital of oxygen atom in COOH group would be dependent whether the COOH group is dissociated or not, however, this is not the case. Therefore, the observed transitions are the $\pi^* \rightarrow \pi$ transitions from the benzene ring of the BDC linker in the A100 MOF and from the benzene ring of BDC in any form.

To support our proposed energy level diagram, we prepared the hydrated A100 sample. Before we measured the fluorescence spectra, we determined the mass change of the non-activated A100 after its thermal activation to form the activated A100. The removal of "free" BDC linkers, adsorbed water and other possible impurities by thermal activation of A100 MOF has caused a decrease of mass at 4.8 wt. %. Subsequently, we determined the mass change of activated A100 after a prolonged hydration procedure in water vapor at RH ~100 % and room temperature (see Experimental). The hydrated A100 obtained after seven days of hydration (7-hyd-A100) was kept in a closed vessel while weighing. The mass increase after hydration indicates an adsorption capacity of four water molecules per one "molecule" of A100 with the nominal formula Al(OH)-BDC. The XRD pattern of the activated A100 is in a good agreement with that of the (*lp*) MIL-53(Al) [28]. Considering the corner-sharing structure of MIL-53(Al), each unit contains four BDC linkers and each BDC linker is shared between two neighboring units. Thus, each structural unit contains two BDC linkers, and the formula of each structural unit

should be written as $(AlOH)_2[BDC]_2$. Based on our determination of 4 adsorbed water molecules per one "molecule" of A100 with nominal formula Al(OH)-BDC, the correct formula of hydrated A100 (7-hyd-A100) is $(AlOH)_2[BDC]_2 (H_2O)_8$. Further, we thermally activated the 7-hyd-A100 following the same procedure as the activation of non-activated A100 (see Experimental). The mass of 7-hyd-A100 decreased by 24 wt. % due to the loss of water, and returns to the original mass with an error of 2%Thus, the activated A100 MOF, $(AlOH)_2[BDC]_2$ was obtained again. When we decreased the hydration time in water vapor to two days, the sample of 2-hyd-A100 with a formula of $(AlOH)_2[BDC]_2 (H_2O)_3$ was obtained according (Figure 17).

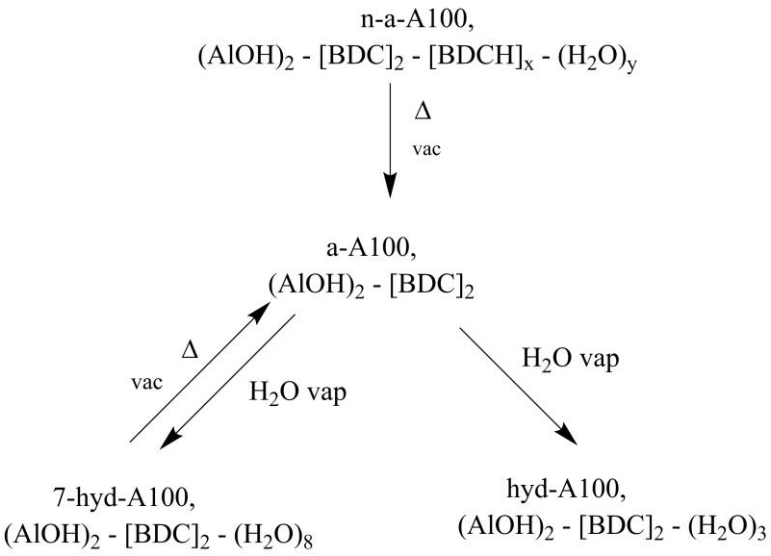

Figure 17. Illustration of activation and different hydration procedures of A100 MOF.

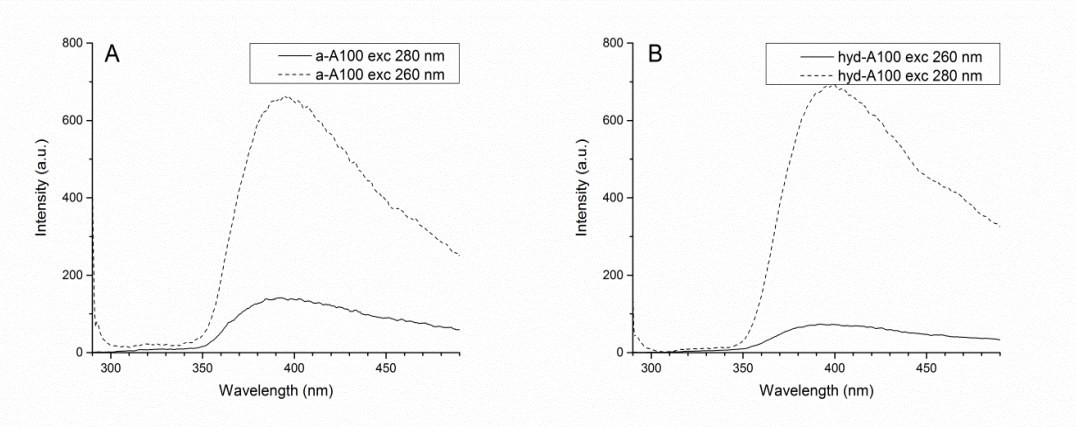

Figure 18. The fluorescence spectra of (A) a-A100 at λ_{exc} = 260 and 280 nm; (B) hyd-A100 at λ_{exc} = 260 and 280 nm.

Next, we measured the wavelength-dependent fluorescence on activated A100 and hydrated A100 (7-hyd-A100). We have obtained the fluorescence spectra of activated A100 at λ_{exc} = 260 nm *vs*. λ_{exc} = 280 nm (Figure 18A), and of hydrated A100 at λ_{exc} = 260 nm *vs*. λ_{exc} = 280 nm (Figure 18B). In all cases, the peak at 320 nm due to the S2 → S0 fluorescence transition is present. We have calculated the relative ratio of the intensity of the emission peak at 400 nm (with intensity I_2) due to the S1 → S0 transition and the peak at 320 nm (with intensity I_2) due to the S2 → S0 transition for both activated A100 and hydrated A100.

For the fluorescence spectra of activated A100 at λ_{exc} = 260 nm and λ_{exc} = 280 nm, the relative ratios of the intensity of peak at 400 nm *vs*. that of peak at 320 nm are R_{exc260} = I_2/I_1 = 16.4, and R_{exc280} = I_2/I_1 = 29.0, respectively. Therefore, for activated A100, excitation at 260 nm yields the higher relative contribution of emission at 320 nm (the low-intensity S2 → S0 transition), compared to the excitation at 280 nm. This is expected, given that the longer wavelength excitation at 280 nm would promote the lower energy S1 → S0 transition, compared to the higher energy transition S2 → S0.

Likewise, for fluorescence spectrum of hydrated A100 at λ_{exc} = 260 nm and λ_{exc} = 280 nm, $R_{exc260} = I_2/I_1 = 14.8$ and $R_{exc280} = I_2/I_1 = 61.5$. This means that photoexcitation of hydrated A100 at 280 nm also gives a higher relative contribution from the peak at 400 nm (the lower energy transition) *vs.* that at 320 nm. Those observations are consistent with the Kasha's rule [92] and the proposed energy diagram with the S0, S1 and S2 levels. Since the fluorescence spectrum of hydrated A100 is almost same as that of the activated A100, we can compare it to the spectrum of activated A100 and propose the energy diagram (Figure 19).

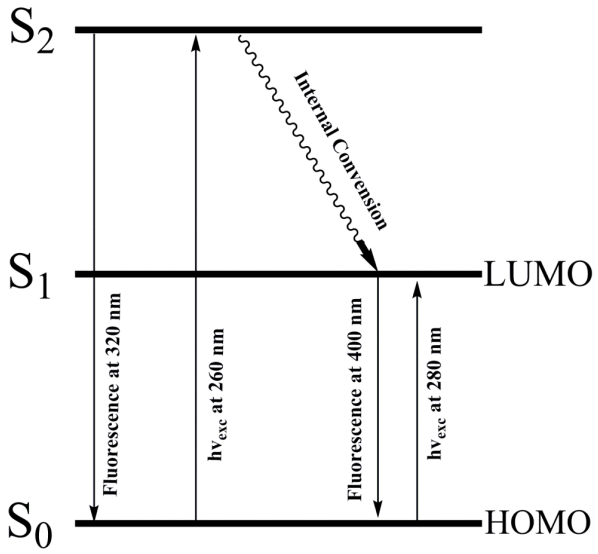

Figure 19. Proposed energy level diagram for the fluorescence of A100 and BDC.

According to our findings above, we proposed that two transitions occur in BDC and A100 MOF. On one hand, the electron in BDC unit is excited to the first singlet state S1 and after vibrational relaxation the photon is emitted at a longer wavelength. In our case, the fluorescence is excited at λ_{exc} = 280 nm the S1 → S0 transition is observed at 400 nm. The excitation slightly off-resonance, compared to the peak in absorption spectrum of BDC in either molecular or anionic form with maximum at 285 nm in Figure 15, is

known to lead to the same shape of the fluorescence spectrum, according to the Kasha-Vavilov rule [93].

On the other hand, the electron might as well be excited to the second singlet state S2 that would correspond to the absorption maximum in the spectrum of BDC at $\lambda = 240$ nm (Figure 15), and the photon is emitted at 400 nm (S1 → S0 transition) after an internal conversion from S2 to S1 state. Nevertheless, a weak emission from S2 → S0 is also possible. In this case, we propose that an excitation close to 240 nm would result in two transitions, S0 → S1 transition and S0 → S2 transition; indeed, with $\lambda_{exc} = 260$ nm, both transitions are excited as judged by two fluorescence peaks at 320 and 400 nm, Figures 16 and 18. The S1 → S0 transition at ca. 285 nm (the absorption maximum of BDC in Figure 15) would be excited at the longer wavelength $\lambda_{exc} = 280$ nm and would cause the S1 → S0 fluorescence transition preferentially, as can be seen in the fluorescence spectra.

In conclusion, the low-intensity emission peak at 320 nm in the fluorescence spectrum of A100 which is assigned by us to the S2 → S0 transition is of higher intensity when excited at the shorter wavelength $\lambda_{exc} = 260$ nm *vs.* $\lambda_{exc} = 280$ nm. On the other hand, excitation at $\lambda_{exc} = 280$ nm would more preferentially effectively result in the S1 → S0 fluorescence transition. The UV-Vis absorption spectra and the fluorescence spectra of BDC in two major forms, and the fluorescence spectra of BDC and A100 MOF supports our hypothesis that the fluorescence of A100 has its origin in the aromatic π-system of phenyl group of BDC linkers.

3.2.2 Fluorescence spectra of A100 and its adsorption complexes with water, indole or naphthalene.

Before we studied the fluorescence of the adsorption complexes of activated A100 with indole or naphthalene, we determined the change of the mass of the activated A100 after the formation of the adsorption "host-guest" complex with either naphthalene or indole. The increase of mass reveals the formula of the adsorption complexes $(AlOH)_2[BDC]_2 \cdot [NAP]_1$ and $(AlOH)_2[BDC_2] \cdot [IND]_1$, respectively. According to the formulae, one naphthalene molecule or one indole molecule is adsorbed per one structural unit in A100 MOF, on average. The kinetic diameter of indole at 5.4 Å [69] is comparable to the micropore size of A100 MOF at 5.3 Å [94]. However, the kinetic diameter of naphthalene molecule at 6.57 Å [95] is larger than the micropore size at 5.3 Å. We speculate that the transformation of the structure of the micropore due to a "breathing" mechanism of A100 occurs to adsorb one naphthalene molecule into the micropore and form the stoichiometric adsorption "host-guest" complex $(AlOH)_2[BDC]_2 \cdot [NAP]_1$.

After we have obtained the stoichiometric adsorption complexes of the activated A100 indole or naphthalene, we studied the mechanisms for adsorption of indole and naphthalene on A100. We first analyzed the fluorescence spectra of the adsorption complexes of indole or naphthalene with activated A100. The spectrum of activated A100 was obtained as a blank. All samples were made and measured in same way according to Experimental section. It is reported that MIL-53(Al) has the maximum fluorescence emission when excited at about 305 nm [25], although the origin of the fluorescence was not reported. In the above section, we have determined the origin of the fluorescence from A100 MOF. As below, we have measured the fluorescence spectra of

A100 and its adsorption complexes with indole or naphthalene at various excitation wavelengths.

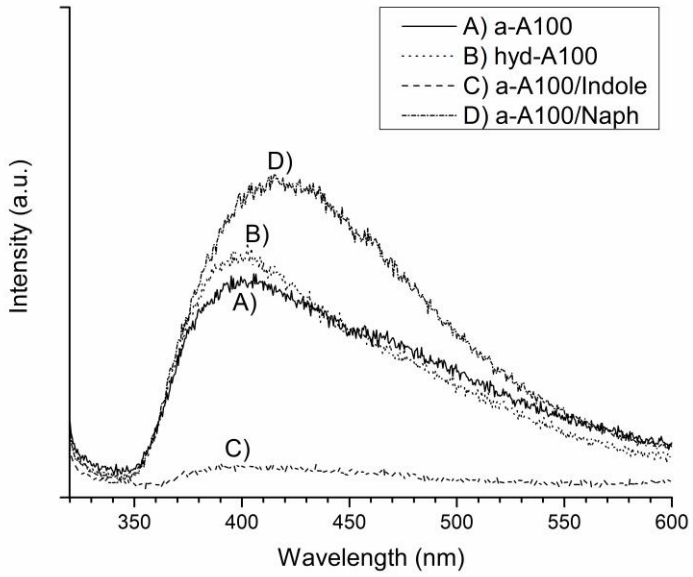

Figure 20: Fluorescence spectra of A) a-A100 at λ_{exc} = 310 nm; B) hydrated A100 at λ_{exc} = 310 nm; C) stoichiometric complex of indole with a-A100 at λ_{exc} = 310 nm; D) stoichiometric complex of naphthalene with a-A100 at λ_{exc} = 310 nm.

First, we have observed a similar shape for all spectra in Figure 20. More specifically, similar broad emission bands are located at 350-600 nm that is consistent with the fluorescence spectra measured by us for A100, Figure 16D and Figure 18. The spectra in Figure 20 are also consistent with fluorescence spectrum for MIL-53(Al) reported by Yang, *et al*. [25] obtained with λ_{exc} = 305 nm. One can see that fluorescence spectra of activated A100 and hydrated A100 are very similar to each other. This means that water adsorbate in hydrated A100 MOF does not significantly change the fluorescence from the electronic states of BDC linker. This is expected, given that adsorbed water forms H-bonding with the COO group of BDC linker, and the COO group does not contribute to

the fluorescence, according to our study of the mechanism of the fluorescence from A100 MOF as provided in previous Section. Based on the fluorescence study of A100, we decided to investigate the fluorescence of adsorption complexes of activated A100 with indole or naphthalene.

Next, we prepared the stoichiometric adsorption complexes of activated A100 with indole or naphthalene, and conducted the fluorescence analysis on these samples. Compared to the spectra in Figure 20A and Figure 20C, we have observed a significant decrease in intensity for activated A100 with indole present in the complex, while the emission band maintains the same shape as that of the activated A100. This suggests quenching of the fluorescence from A100 caused by the adsorption of indole. Because the Al cluster in A100 MOF does not have available CUS, we suggest an adsorption by the π-π interaction between indole molecules and phenyl groups of BDC linkers in A100.

In contrast with the spectrum of the adsorption complex of activated A100 with indole, the spectrum of the stoichiometric "host-guest" adsorption complex of the activated A100 with naphthalene (Figure 20D) is rather a different case. Namely, a red shift of emission peak from 410 nm to 420 nm is observed, and there is also an increase in intensity. However, it is difficult to determine whether the change of the spectrum originates from the electronic interaction between naphthalene and A100 or just from an overlap with the fluorescence emission from adsorbed naphthalene with that of A100. Since indole and naphthalene are known to have absorption bands at 250-300 nm, the excitation at 372 nm would give us the fluorescence spectrum of A100 free from the contribution of the fluorescence of naphthalene or indole. In order to verify the fluorescence quenching caused by the indole adsorbate, we shifted the excitation

wavelength to the red, and further examined the fluorescence spectra of the stoichiometric adsorption complexes of activated A100 with indole or naphthalene at λ_{exc} = 372 nm.

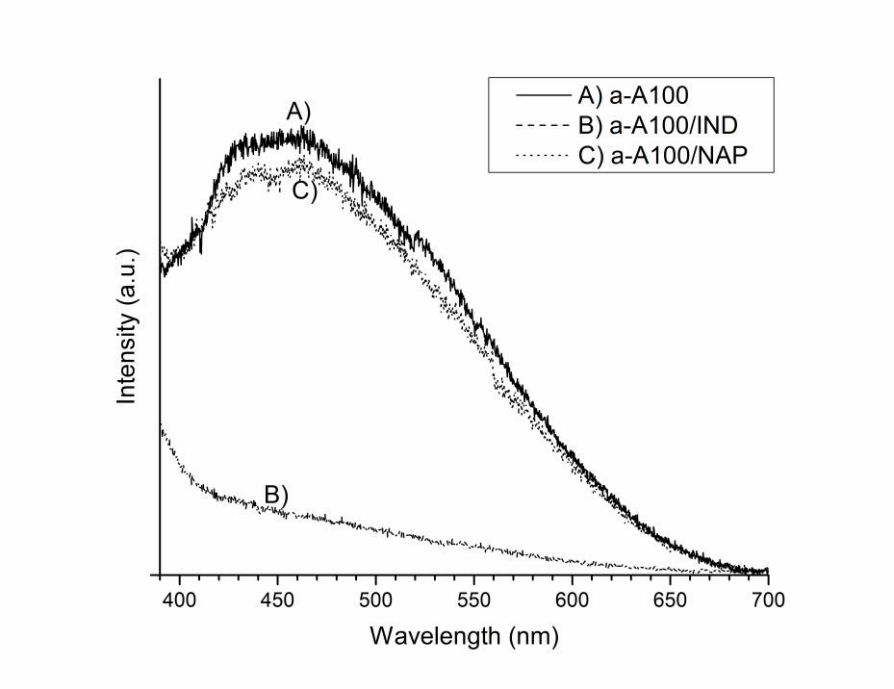

Figure 21. Fluorescence spectra at λ_{exc} = 372 nm of A) a-A100; B) stoichiometric complex of indole with a-A100; C) stoichiometric complex of naphthalene with a-A100.

After formation of the adsorption complex with indole, the intensity of the emission band of A100 MOF at 400-700 nm decreases significantly this indicates fluorescence quenching, and therefore confirms our observation of quenching due to adsorption of indole. Further, we found the major difference between the fluorescence spectrum of adsorption complex of activated A100 with naphthalene at λ_{exc} = 310 nm (Figure 20D) and that at λ_{exc} = 372 nm (Figure 21C). Instead of the higher intensity of the fluorescence spectrum of adsorption complex of A100 and naphthalene compared to that of A100 at λ_{exc} = 310 nm (Figure 20D), we observed a slight reduction in intensity of the emission at 400-700 nm for the adsorption complex *vs*. A100 at λ_{exc} = 372 nm in Figure 21C, while

the fluorescence spectrum of adsorption complex of activated A100 with naphthalene has maintained a similar shape and intensity to that of activated A100 (Figure 21A). This can be explained by the absence of the fluorescence of naphthalene at λ_{exc} = 372 nm and some quenching of the fluorescence of A100, although in much weaker extent than that observed with indole as adsorbate. Similarly, we suggest that the adsorption of naphthalene by the π-π interaction with the π-system of phenyl group of the BDC linker in A100 MOF causes the quenching of fluorescence of A100.

3.2.3 Fluorescence analysis of electronic interaction between BDC and indole

In our mechanistic studies of the origin of the fluorescence from BDC linker in A100 MOF, we used liquid solution as the model system. We decided to perform the fluorescence analysis on binary solution of BDC and indole in DMF, since our study on the fluorescence spectrum of A100 and adsorption complexes of A100 with indole or naphthalene has suggested a ligand-based fluorescence in A100. We hypothesized above that the fluorescence of A100 is from the phenyl group in BDC linker. In this case, the similar π-π interaction would exist in a mixture of BDC and indole as well, and it would cause quenching of the fluorescence from BDC. To justify our hypothesis, we prepared the binary stoichiometric solution of BDC and indole in DMF and obtained the fluorescence spectrum.

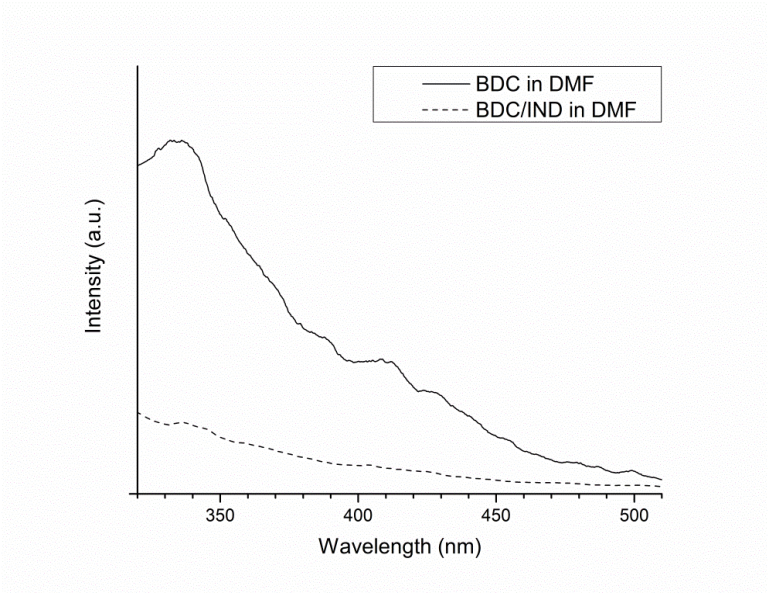

Figure 22. Fluorescence spectra of 0.08 M solution of BDC in DMF and 0.08 M binary solution of BDC and indole in DMF at λexc = 310 nm.

We first obtained the fluorescence spectrum of 0.08 M solution BDC in DMF (Figure 22), and we observed an emission band with maximum at 336 nm and a shoulder at 410 nm. Next, we dissolved a stoichiometric amount of indole in that 0.08 M solution of BDC in DMF to make the 1:1 stoichiometric binary solution. A significant decrease in intensity was observed the binary solution, while the spectral shape remained the same. This indicates fluorescence quenching caused by the π-π interaction between BDC and indole. In solution, the fluorescence quenching of the excited state of the π-π complexes is well known, including the "exciplex" containing indole and benzene [86]. Thus, our hypothesis of quenching of the emission from the π-π system of BDC linker in A100 MOF is confirmed by the independent measurement in the model solution. Therefore, the fluorescence of the adsorption complex of activated A100 has its origin in the molecular orbitals of the aromatic system of the phenyl group of BDC linkers, and the adsorption of indole onto activated A100 by the π-π interaction quenches the fluorescence quenching of

A100. Our proposed scheme of quenching in fluorescence of activated A100 is shown as followed:

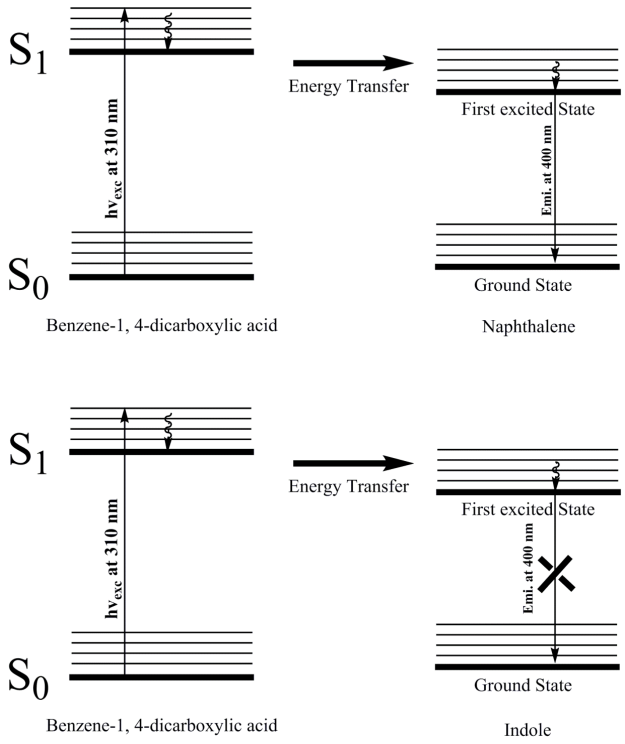

Figure 23. Proposed fluorescence quenching in the adsorption complexes of A100 MOF with naphthalene (top) and indole (bottom).

As shown in Figure 23, we propose that phenyl group in BDC linkers of A100 is excited to the first singlet state at λ_{exc} = 310 nm and the excitation energy is then transferred within this π-π adsorption complex to the naphthalene or indole unit in this complex. In the adsorption complex of activated A100 with naphthalene, the emission is due to a first excited state to ground state transition. The fluorescence emission of the stoichiometric adsorption complex of activated A100 with naphthalene at 400 nm that was observed at λ_{exc} = 310 nm (naphthalene does not absorb light) is of a lesser intensity than that in activated A100, due to some energy loss during energy transfer from BDC to adsorbed naphthalene. It is different in the stoichiometric adsorption complex of activated

A100 with indole. When energy is transferred to adsorbed indole from the excited state in the BDC linker, the emission at 400 nm is strongly quenched, since energy is transferred to indole that has a weak fluorescence. The weak emission from indole is attributed to the intersystem crossing that is due to the spin-orbit coupling in the aromatic heterocyclic compounds as compared to aromatic hydrocarbons [96]. Thus, indole and naphthalene are adsorbed onto A100 through the π-π interaction with aromatic system of BDC linker, and quench the fluorescence of A100, although in a different amount. Further investigation on the quenching mechanism by indole is in progress.

3.2.4 Fluorescence of stoichiometric adsorption complexes of A100 under UV lamp

To visualize the quenching of the fluorescence of A100, the image of the fluorescence of the stoichiometric adsorption complexes of A100 with indole and naphthalene was obtained under the UV lamp. Pictures were taken by digital camera under a UV radiation lamp (see Experimental) at 254 nm and 312 nm, and no manipulation was performed with original digital pictures. Figure S4 (see the Supplementary) shows the fluorescence images of those adsorption complexes. Only the stoichiometric adsorption complex of activated A100 with indole shows no fluorescence as seen by naked eye that is different from the activated A100 and stoichiometric adsorption complex of activated A100 with naphthalene that emit visible light under the UV absorption. The visible fluorescence in Figure S3 (see supplementary) is consistent with visible fluorescence at λ>400 nm from A100 as in the fluorescence spectra from A100 and its adsorption complexes with water, indole and naphthalene, Figure 20.

4 Conclusions

We have studied the adsorption of a prototype fused-ring N-heterocyclic compound, namely indole, and a fused-ring aromatic hydrocarbon, namely naphthalene, on a microporous MOF without CUS, i.e., A100 and on mesoporous MOFs with the CUS, i.e., F300 MOF and MIL-100(Fe). We have the following major findings.

In the research with the mesoporous MOFs with Fe^{3+} CUS, we have detected the formation of the coordination complex between indole and Fe^{3+} CUS in F300 by near-UV/Vis diffuse reflectance spectroscopy, wavelength-dependent fluorescence spectroscopy and time-dependent fluorescence spectroscopy. Indole is weakly electronically bound to Fe^{3+} CUS in F300 and MIL-100(Fe) in the adsorption complex, and the presence of molar excess of indole is necessary to spectroscopically detect this complex. On the other hand, the confinement of adsorbed naphthalene in the meso-cavity of F300 MOF was demonstrated by the vibronically-resolved fluorescence spectroscopy for the first time. These results are also published in the paper "Adsorption of naphthalene and indole on F300 MOF in liquid phase by the complementary spectroscopic, kinetic and DFT studies" in the Journal of Porous Materials [97].

In our research with the microporous MOF without CUS, A100 we have determined the origin of the near-UV and visible fluorescence from A100 as the emission from the aromatic system of the phenyl ring of the BDC linker, using two methods of molecular spectroscopy. The 1:1 stoichiometric adsorption complexes of activated A100 MOF with indole and naphthalene were obtained. The nature of bonding of the indole *vs.* naphthalene to adsorption sites in A100 MOF in the stoichiometric adsorption complexes was studied spectroscopically. Both adsorption complexes are formed by the π-π

interactions between the BDC linker in A100 MOF and heteroaromatic or aromatic system of indole and naphthalene adsorbate, respectively. The significant quenching on fluorescence of A100 due to the adsorption of indole is due to the π-π interaction with the phenyl group of BDC linker.

5 Future Plans

As was determined by us for the activated F300 MOF, the adsorption of indole is due to coordination bonding to the Fe^{3+} CUS. At the same time, co-adsorption of indole and naphthalene from solution on activated MIL-100(Fe) of the similar structure was found. This indicates that the coordination bonding to the CUS is not sufficient to obtain the selective adsorption of the fused-ring aromatic N-heterocyclic compounds from petroleum and liquid fuels, such as indole, in the presence of the fused ring aromatic hydrocarbons such as naphthalene. Therefore, the alternative mechanism of the selective adsorption needs to be studied. Specifically, we detected the formation of hydrated A100 MOF with a large molar amount of adsorbed water. In the plans are the preparation of hydrated F300 and MIL-100(Fe) MOFs and the mechanistic studies on the stoichiometry and stability of their adsorption complexes with indole and naphthalene, and major kinds of chemical bonding in these complexes. The stability and stoichiometry of the adsorption complexes of the MOFs with pre-adsorbed water would be indicative of whether the preferential adsorption of either adsorbate onto hydrated MOFs with CUS would occur. Instead of pre-adsorbed water, some other highly polar small molecule compounds can be pre-adsorbed onto the CUS in order to utilize hydrogen bonding with the adsorbate. This hydrogen bonding is expected to be selective towards heterocyclic compounds in the presence of aromatic hydrocarbons of the similar molecular size.

Further, we have detected a significant molar amount of pre-adsorbed water on A100 MOF. In the plans, the selectivity of adsorption of indole in the presence of naphthalene on the hydrated MOFs without the CUS, such as hydrated A100 MOF and MIL-53(Al) will need to be investigated. This proposal is based on the alternative mechanism of

adsorption: via hydrogen bonding instead of π-π bonding. Further, a strong and selective hydrogen bonding could be obtained with polar indole *vs*. nonpolar naphthalene adsorbate, even in the presence of the competing π-π bonding that is non-selective based on our data. Specifically, the strong hydrogen bonding can be obtained using A100 and similar MOFs with pre-adsorbed small polar molecules other than water.

References

(1) Pan, L.; Sander, M. B.; Huang, X.; Li, J.; Smith, M.; Bittner, E.; Bockrath, B.; Johnson, J. K. Microporous Metal Organic Materials: Promising Candidates as Sorbents for Hydrogen Storage. *J. Am. Chem. Soc.* **2004**, *126*, 1308–1309.

(2) Yoon, J. W.; Seo, Y.-K.; Hwang, Y. K.; Chang, J.-S.; Leclerc, H.; Wuttke, S.; Bazin, P.; Vimont, A.; Daturi, M.; Bloch, E.; Llewellyn, P. L.; Serre, C.; Horcajada, P.; Grenèche, J.-M.; Rodrigues, A. E.; Férey, G. Controlled Reducibility of a Metal-Organic Framework with Coordinatively Unsaturated Sites for Preferential Gas Sorption. *Angew. Chem. Int. Ed. Engl.* **2010**, *49*, 5949–5952.

(3) Li, Z.-Q.; Qiu, L.-G.; Wang, W.; Xu, T.; Wu, Y.; Jiang, X. Fabrication of Nanosheets of a Fluorescent Metal–organic Framework [Zn(BDC)(H2O)]n (BDC=1,4-Benzenedicarboxylate): Ultrasonic Synthesis and Sensing of Ethylamine. *Inorg. Chem. Commun.* **2008**, *11*, 1375–1377.

(4) Yang, K.; Sun, Q.; Xue, F.; Lin, D. Adsorption of Volatile Organic Compounds by Metal-Organic Frameworks MIL-101: Influence of Molecular Size and Shape. *J. Hazard. Mater.* **2011**, *195*, 124–131.

(5) Wade, C. R.; Dincă, M. Investigation of the Synthesis, Activation, and Isosteric Heats of CO2 Adsorption of the Isostructural Series of Metal-Organic Frameworks M3(BTC)2 (M = Cr, Fe, Ni, Cu, Mo, Ru). *Dalton Trans.* **2012**, *41*, 7931–7938.

(6) Münch, A. S.; Mertens, F. O. R. L. HKUST-1 as an Open Metal Site Gas Chromatographic Stationary Phase—capillary Preparation, Separation of Small Hydrocarbons and Electron Donating Compounds, Determination of Thermodynamic Data. *J. Mater. Chem.* **2012**, *22*, 10228–10234.

(7) Borfecchia, E.; Maurelli, S. Insights into Adsorption of NH3 on HKUST-1 Metal–Organic Framework: A Multitechnique Approach. *J. Phys. Chem. C* **2012**, *116*, 19839–19850.

(8) Petit, C.; Bandosz, T. J. Synthesis, Characterization, and Ammonia Adsorption Properties of Mesoporous Metal-Organic Framework (MIL(Fe))-Graphite Oxide Composites: Exploring the Limits of Materials Fabrication. *Adv. Funct. Mater.* **2011**, *21*, 2108–2117.

(9) Klein, N.; Senkovska, I.; Gedrich, K.; Stoeck, U.; Henschel, A.; Mueller, U.; Kaskel, S. A Mesoporous Metal-Organic Framework. *Angew. Chem. Int. Ed. Engl.* **2009**, *48*, 9954–9957.

(10) Karra, J. R.; Walton, K. S. Effect of Open Metal Sites on Adsorption of Polar and Nonpolar Molecules in Metal-Organic Framework Cu-BTC. *Langmuir* **2008**, *24*, 8620–8626.

(11) Schlichte, K.; Kratzke, T.; Kaskel, S. Improved Synthesis, Thermal Stability and Catalytic Properties of the Metal-Organic Framework Compound Cu3(BTC)2. *Microporous Mesoporous Mater.* **2004**, *73*, 81–88.

(12) Loiseau, T.; Serre, C.; Huguenard, C.; Fink, G.; Taulelle, F.; Henry, M.; Bataille, T.; Férey, G. A Rationale for the Large Breathing of the Porous Aluminum Terephthalate (MIL-53) upon Hydration. *Chemistry* **2004**, *10*, 1373–1382.

(13) Huo, S.-H.; Yan, X.-P. Facile Magnetization of Metal-Organic Framework MIL-101 for Magnetic Solid-Phase Extraction of Polycyclic Aromatic Hydrocarbons in Environmental Water Samples. *Analyst* **2012**, *137*, 3445–3451.

(14) Dhakshinamoorthy, A.; Alvaro, M.; Horcajada, P.; Gibson, E.; Vishnuvarthan, M.; Vimont, A.; Grenèche, J.-M.; Serre, C.; Daturi, M.; Garcia, H. Comparison of Porous Iron Trimesates Basolite F300 and MIL-100 (Fe) as Heterogeneous Catalysts for Lewis Acid and Oxidation Reactions: Roles of Structural Defects and Stability. *ACS Catal.* **2012**, *100*, 2060–2065.

(15) Horcajada, P.; Surblé, S.; Serre, C.; Hong, D.-Y.; Seo, Y.-K.; Chang, J.-S.; Grenèche, J.-M.; Margiolaki, I.; Férey, G. Synthesis and Catalytic Properties of MIL-100(Fe), an iron(III) Carboxylate with Large Pores. *Chem. Commun. (Camb).* **2007**, *100*, 2820–2822.

(16) Xiang, S.; Zhou, W.; Zhang, Z.; Green, M. a; Liu, Y.; Chen, B. Open Metal Sites within Isostructural Metal-Organic Frameworks for Differential Recognition of Acetylene and Extraordinarily High Acetylene Storage Capacity at Room Temperature. *Angew. Chem. Int. Ed. Engl.* **2010**, *49*, 4615–4618.

(17) Maes, M.; Trekels, M.; Boulhout, M.; Schouteden, S.; Vermoortele, F.; Alaerts, L.; Heurtaux, D.; Seo, Y.-K.; Hwang, Y. K.; Chang, J.-S.; Beurroies, I.; Denoyel, R.; Temst, K.; Vantomme, A.; Horcajada, P.; Serre, C.; De Vos, D. E. Selective Removal of N-Heterocyclic Aromatic Contaminants from Fuels by Lewis Acidic Metal-Organic Frameworks. *Angew. Chem. Int. Ed. Engl.* **2011**, *50*, 4210–4214.

(18) Ahmed, I.; Hasan, Z.; Khan, N. A.; Jhung, S. H. Adsorptive Denitrogenation of Model Fuels with Porous Metal-Organic Frameworks (MOFs): Effect of Acidity and Basicity of MOFs. *Appl. Catal. B Environ.* **2013**, *129*, 123–129.

(19) Coudert, F.-X.; Ortiz, A. U.; Haigis, V.; Bousquet, D.; Fuchs, A. H.; Ballandras, A.; Weber, G.; Bezverkhyy, I.; Geoffroy, N.; Bellat, J.-P.; Ortiz, G.; Chaplais, G.; Patarin, J.; Boutin, A. Water Adsorption in Flexible Gallium-Based MIL-53 Metal–Organic Framework. *J. Phys. Chem. C* **2014**, *118*, 5397–5405.

(20) Horcajada, P.; Chalati, T.; Serre, C.; Gillet, B.; Sebrie, C.; Baati, T.; Eubank, J. F.; Heurtaux, D.; Clayette, P.; Kreuz, C.; Chang, J.-S.; Hwang, Y. K.; Marsaud, V.; Bories, P.-N.; Cynober, L.; Gil, S.; Férey, G.; Couvreur, P.; Gref, R. Porous Metal-Organic-Framework Nanoscale Carriers as a Potential Platform for Drug Delivery and Imaging. *Nat. Mater.* **2010**, *9*, 172–178.

(21) Gaab, M.; Trukhan, N.; Maurer, S.; Gummaraju, R.; Müller, U. The Progression of Al-Based Metal-Organic Frameworks – From Academic Research to Industrial Production and Applications. *Microporous Mesoporous Mater.* **2012**, *157*, 131–136.

(22) Llewellyn, P. L.; Bourrelly, S.; Serre, C.; Filinchuk, Y.; Férey, G. How Hydration Drastically Improves Adsorption Selectivity for CO(2) over CH(4) in the Flexible Chromium Terephthalate MIL-53. *Angew. Chem. Int. Ed. Engl.* **2006**, *45*, 7751–7754.

(23) Gordon, J.; Kazemian, H.; Rohani, S. Rapid and Efficient Crystallization of MIL-53(Fe) by Ultrasound and Microwave Irradiation. *Microporous Mesoporous Mater.* **2012**, *162*, 36–43.

(24) Chen, L.; Mowat, J. P. S.; Fairen-Jimenez, D.; Morrison, C. A.; Thompson, S. P.; Wright, P. A.; Düren, T. Elucidating the Breathing of the Metal-Organic Framework MIL-53(Sc) with Ab Initio Molecular Dynamics Simulations and in Situ X-Ray Powder Diffraction Experiments. *J. Am. Chem. Soc.* **2013**, *135*, 15763–15773.

(25) Yang, C.-X.; Ren, H.-B.; Yan, X.-P. Fluorescent Metal-Organic Framework MIL-53(Al) for Highly Selective and Sensitive Detection of Fe3+ in Aqueous Solution. *Anal. Chem.* **2013**, *85*, 7441–7446.

(26) Horcajada, P.; Serre, C.; Vallet-Regí, M.; Sebban, M.; Taulelle, F.; Férey, G. Metal-Organic Frameworks as Efficient Materials for Drug Delivery. *Angew. Chem. Int. Ed. Engl.* **2006**, *45*, 5974–5978.

(27) Rallapalli, P.; Patil, D.; Prasanth, K. P.; Somani, R. S.; Jasra, R. V.; Bajaj, H. C. An Alternative Activation Method for the Enhancement of Methane Storage Capacity of Nanoporous Aluminium Terephthalate, MIL-53(Al). *J. Porous Mater.* **2009**, *17*, 523–528.

(28) Möllmer, J.; Lange, M.; Möller, A.; Patzschke, C.; Stein, K.; Lässig, D.; Lincke, J.; Gläser, R.; Krautscheid, H.; Staudt, R. Pure and Mixed Gas Adsorption of CH4 and N2 on the Metal–organic Framework Basolite® A100 and a Novel Copper-Based 1,2,4-Triazolyl Isophthalate MOF. *J. Mater. Chem.* **2012**, *22*, 10274–10286.

(29) Blanco-Brieva, G.; Campos-Martin, J. M.; Al-Zahrani, S. M.; Fierro, J. L. G. Effectiveness of Metal–organic Frameworks for Removal of Refractory Organo-Sulfur Compound Present in Liquid Fuels. *Fuel* **2011**, *90*, 190–197.

(30) Tseng, C.-Y.; Huang, Y.-C.; Su, S.-Y.; Huang, J.-Y.; Lai, C.-H.; Lung, C.-C.; Ho, C.-C.; Liaw, Y.-P. Cell Type Specificity of Female Lung Cancer Associated with Sulfur Dioxide from Air Pollutants in Taiwan: An Ecological Study. *BMC Public Health* **2012**, *12*, 4.

(31) Wei, Y.; Davis, J.; Bina, W. F. Ambient Air Pollution Is Associated with the Increased Incidence of Breast Cancer in US. *Int. J. Environ. Health Res.* **2012**, *22*, 12–21.

(32) Jayaraman, A.; Yang, F. H.; Yang, R. T. Effects of Nitrogen Compounds and Polyaromatic Hydrocarbons on Desulfurization of Liquid Fuels by Adsorption via Π -Complexation with Cu (I) Y Zeolite. *Energy & Fuels* **2006**, *20*, 909–914.

(33) Song, C. An Overview of New Approaches to Deep Desulfurization for Ultra-Clean Gasoline, Diesel Fuel and Jet Fuel. *Catal. Today* **2003**, *86*, 211–263.

(34) Zeuthen, P.; Knudsen, K. G.; Whitehurst, D. D. Organic Nitrogen Compounds in Gas Oil Blends, Their Hydrotreated Products and the Importance to Hydrotreatment. *Catal. Today* **2001**, *65*, 307–314.

(35) Ho, T. C. Property–reactivity Correlation for HDS of Middle Distillates. *Appl. Catal. A Gen.* **2003**, *244*, 115–128.

(36) Laredo, G. C.; Altamirano, E.; De los Reyes, J. A. Inhibition Effects of Nitrogen Compounds on the Hydrodesulfurization of Dibenzothiophene: Part 2. *Appl. Catal. A Gen.* **2003**, *243*, 207–214.

(37) Shin, S.; Yang, H.; Sakanishi, K.; Mochida, I.; Grudoski, D. A.; Shinn, J. H. Inhibition and Deactivation in Staged Hydrodenitrogenation and Hydrodesulfurization of Medium Cycle Oil over NiMoS/Al2O3 Catalyst. *Appl. Catal. A Gen.* **2001**, *205*, 101–108.

(38) Kaernbach, W.; Kisielow, W.; Warzecha, L.; Miga, K.; Klecan, R. Influence of Petroleum Nitrogen Compounds on Hydrodesulphurization. *Fuel* **1990**, *69*, 221–224.

(39) Macaud, M.; Sévignon, M.; Favre-Réguillon, A.; Lemaire, M.; Schulz, E.; Vrinat, M. Novel Methodology toward Deep Desulfurization of Diesel Feed Based on the Selective Elimination of Nitrogen Compounds. *Ind. Eng. Chem. Res.* **2004**, *43*, 7843–7849.

(40) Anderson, B.; Bartlett, K.; Frolking, S.; Hayhoe, K. *Methane and Nitrous Oxide Emissions from Natural Sources*; Washington, 2010; pp. 1–2.

(41) U.S. environmental protection agency. Air Trends Summary Report http://www.epa.gov/airtrends/2011/ (accessed Sep 3, 2014).

(42) Benedik, M. J.; Gibbs, P. R.; Riddle, R. R.; Willson, R. C. Microbial Denitrogenation of Fossil Fuels. *Trends Biotechnol.* **1998**, *16*, 390–395.

(43) Microbial Metabolism of Quinoline and Related Compounds. IV. Degradation of Isoquinoline by Alcaligenes Faecalis Pa and Pseudomonas Diminuta 7. *Biol. Chem. Hoppe. Seyler.* **1990**, *371*, 511–513.

(44) Ouchiyama, N.; Zhang, Y.; Omori, T.; Kodama, T. Biodegradation of Carbazole by Pseudomonas Spp. CA06 and CA10. *Biosci. Biotechnol. Biochem.* **1993**, *57*, 455–460.

(45) Hisatsuka, K.; Sato, M. Microbial Transformation of Carbazole to Anthranilic Acid by Pseudomonas Stutzeri. *Biosci. Biotechnol. Biochem.* **1994**, *58*, 213–214.

(46) Kaiser, J. P.; Feng, Y.; Bollag, J. M. Microbial Metabolism of Pyridine, Quinoline, Acridine, and Their Derivatives under Aerobic and Anaerobic Conditions. *Microbiol. Rev.* **1996**, *60*, 483–498.

(47) Sumbogo Murti, S. D.; Yang, H.; Choi, K.-H.; Korai, Y.; Mochida, I. Influences of Nitrogen Species on the Hydrodesulfurization Reactivity of a Gas Oil over Sulfide Catalysts of Variable Activity. *Appl. Catal. A Gen.* **2003**, *252*, 331–346.

(48) Choi, K.-H.; Korai, Y.; Mochida, I.; Ryu, J.-W.; Min, W. Impact of Removal Extent of Nitrogen Species in Gas Oil on Its HDS Performance: An Efficient Approach to Its Ultra Deep Desulfurization. *Appl. Catal. B Environ.* **2004**, *50*, 9–16.

(49) Macaud, M. Novel Methodology toward Deep Desulfurization of Diesel Feed Based on the Selective Elimination of Nitrogen Compounds. *Ind. Eng. Chem. Res.* **2004**, *43*, 7843–7849.

(50) Almarri, M.; Ma, X.; Song, C. Selective Adsorption for Removal of Nitrogen Compounds from Liquid Hydrocarbon Streams over Carbon- and Alumina-Based Adsorbents. *Ind. Eng. Chem. Res.* **2009**, *48*, 951–960.

(51) Almarri, M.; Ma, X.; Song, C. Role of Surface Oxygen-Containing Functional Groups in Liquid-Phase Adsorption of Nitrogen Compounds on Carbon-Based Adsorbents. *Energy & Fuels* **2009**, *23*, 3940–3947.

(52) Sano, Y.; Choi, K.-H.; Korai, Y.; Mochida, I. Selection and Further Activation of Activated Carbons for Removal of Nitrogen Species in Gas Oil as a Pretreatment for Its Deep Hydrodesulfurization. *Energy & Fuels* **2004**, *18*, 644–651.

(53) Sano, Y.; Choi, K.-H.; Korai, Y.; Mochida, I. Adsorptive Removal of Sulfur and Nitrogen Species from a Straight Run Gas Oil over Activated Carbons for Its Deep Hydrodesulfurization. *Appl. Catal. B Environ.* **2004**, *49*, 219–225.

(54) Liu, D.; Gui, J.; Sun, Z. Adsorption Structures of Heterocyclic Nitrogen Compounds over Cu(I)Y Zeolite: A First Principle Study on Mechanism of the Denitrogenation and the Effect of Nitrogen Compounds on Adsorptive Desulfurization. *J. Mol. Catal. A Chem.* **2008**, *291*, 17–21.

(55) Audeh, C. A. Removal of Nitrogen Compounds from Lubricating Oils. *Ind. Eng. Chem. Prod. Res. Dev.* **1983**, *22*, 276–279.

(56) Xie, L.-L.; Favre-Reguillon, A.; Wang, X.-X.; Fu, X.; Lemaire, M. Selective Adsorption of Neutral Nitrogen Compounds from Fuel Using Ion-Exchange Resins. *J. Chem. Eng. Data* **2010**, *55*, 4849–4853.

(57) Kwon, J.-M.; Moon, J.-H.; Bae, Y.-S.; Lee, D.-G.; Sohn, H.-C.; Lee, C.-H. Adsorptive Desulfurization and Denitrogenation of Refinery Fuels Using Mesoporous Silica Adsorbents. *ChemSusChem* **2008**, *1*, 307–309.

(58) Koriakin, A.; Ponvel, K. M.; Lee, C.-H. Denitrogenation of Raw Diesel Fuel by Lithium-Modified Mesoporous Silica. *Chem. Eng. J.* **2010**, *162*, 649–655.

(59) Zhang, H.; Li, G.; Jia, Y.; Liu, H. Adsorptive Removal of Nitrogen-Containing Compounds from Fuel. *J. Chem. Eng. Data* **2010**, *55*, 173–177.

(60) Sun, B.; Li, G.; Wang, X. Facile Synthesis of Microporous Carbon through a Soft-Template Pathway and Its Performance in Desulfurization and Denitrogenation. *J. Nat. Gas Chem.* **2010**, *19*, 471–476.

(61) Kim, J. H.; Ma, X.; Zhou, A.; Song, C. Ultra-Deep Desulfurization and Denitrogenation of Diesel Fuel by Selective Adsorption over Three Different Adsorbents: A Study on Adsorptive Selectivity and Mechanism. *Catal. Today* **2006**, *111*, 74–83.

(62) Sun, M.; Nelson, A. E.; Adjaye, J. First Principles Study of Heavy Oil Organonitrogen Adsorption on NiMoS Hydrotreating Catalysts. *Catal. Today* **2005**, *109*, 49–53.

(63) Maes, M.; Vermoortele, F.; Boulhout, M.; Boudewijns, T.; Kirschhock, C.; Ameloot, R.; Beurroies, I.; Denoyel, R.; De Vos, D. E. Enthalpic Effects in the

Adsorption of Alkylaromatics on the Metal-Organic Frameworks MIL-47 and MIL-53. *Microporous Mesoporous Mater.* **2012**, *157*, 82–88.

(64) Henschel, A.; Senkovska, I.; Kaskel, S. Liquid-Phase Adsorption on Metal-Organic Frameworks. *Adsorption* **2011**, *17*, 219–226.

(65) Nuzhdin, A. L.; Kovalenko, K. a.; Dybtsev, D. N.; Bukhtiyarova, G. a. Removal of Nitrogen Compounds from Liquid Hydrocarbon Streams by Selective Sorption on Metal-Organic Framework MIL-101. *Mendeleev Commun.* **2010**, *20*, 57–58.

(66) Leclerc, H.; Vimont, A.; Lavalley, J.-C.; Daturi, M.; Wiersum, A. D.; Llwellyn, P. L.; Horcajada, P.; Férey, G.; Serre, C. Infrared Study of the Influence of Reducible iron(III) Metal Sites on the Adsorption of CO, CO2, Propane, Propene and Propyne in the Mesoporous Metal-Organic Framework MIL-100. *Phys. Chem. Chem. Phys.* **2011**, *13*, 11748–11756.

(67) Shan, G.; Liu, H.; Xing, J.; Zhang, G.; Wang, K. Separation of Polycyclic Aromatic Compounds from Model Gasoline by Magnetic Alumina Sorbent Based on Π-Complexation. *Ind. Eng. Chem. Res.* **2004**, *43*, 758–761.

(68) Centrone, A.; Santiso, E. E.; Hatton, T. A. Separation of Chemical Reaction Intermediates by Metal-Organic Frameworks. *Small* **2011**, *7*, 2356–2364.

(69) Zhang, H.; Li, G.; Jia, Y.; Liu, H. Adsorptive Removal of Nitrogen-Containing Compounds from Fuel. *J. Chem. Eng. Data* **2010**, *55*, 173–177.

(70) Allendorf, M. D.; Bauer, C. a; Bhakta, R. K.; Houk, R. J. T. Luminescent Metal-Organic Frameworks. *Chem. Soc. Rev.* **2009**, *38*, 1330–1352.

(71) Patil, S.; Patwari, S. Red Shift in Fluorescence of Naphthalene Doped by Anthracene and Perylene. *J. Lumin.* **1999**, *82*, 115–119.

(72) Lakowicz, J. R. *Principles of Fluorescence Spectroscopy*; Springer Science & Business Media, 2006; pp. 27–31.

(73) Singh, D.; Chopra, A.; Patel, M. B.; Sarpal, A. S. A Comparative Evaluation of Nitrogen Compounds in Petroleum Distillates. *Chromatographia* **2011**, *74*, 121–126.

(74) Privalova, A. I.; Morozova, J. P.; Kashapova, E. R.; Artyukhov, V. J. Spectral and Luminescent Properties of 1-Substituted Naphthalenes. *J. Appl. Spectrosc.* **2011**, *78*, 309–317.

(75) Schnepp, O.; McClure, D. S. A Vibrational Analysis of the Fluorescence of Naphthalene Vapor. *J. Chem. Phys.* **1952**, *20*, 1375–1383.

(76) Prahl, S. Naphthalene http://omlc.org/spectra/PhotochemCAD/html/001.html (accessed Aug 29, 2014).

(77) Behlen, F. M.; MacDonald, D. B.; Sethuraman, V.; Rice, S. A. Fluorescence Spectroscopy of Cold and Warm Naphthalene Molecules: Some New Vibrational Assignments. *J. Chem. Phys.* **1981**, *75*, 5685–5693.

(78) Hochstrasser, R. The Luminescence of Organic Molecular Crystals. *Rev. Mod. Phys.* **1962**, *34*, 531–550.

(79) Berlman, I. B.; Weinreb, A. On the Fluorescence Spectrum and Decay Time of Naphthalene. *Mol. Phys.* **1962**, *5*, 313–319.

(80) Zhang, Z.; Long, J.; Xie, X.; Lin, H.; Zhou, Y.; Yuan, R.; Dai, W.; Ding, Z.; Wang, X.; Fu, X. Probing the Electronic Structure and Photoactivation Process of Nitrogen-Doped TiO2 Using DRS, PL, and EPR. *ChemPhysChem* **2012**, *13*, 1542–1550.

(81) Aladekomo, J. B.; Birks, J. B. "Excimer" Fluorescence. VII. Spectral Studies of Naphthalene and Its Derivatives. *Proc. R. Soc. A Math. Phys. Eng. Sci.* **1965**, *284*, 551–565.

(82) Smith, F. J.; Armstrong, A. T.; McGlynn, S. P. Energy of Excimer Luminescence. V. Excimer Fluorescence of Naphthalene and Methylnaphthalenes. *J. Chem. Phys.* **1966**, *44*, 442–448.

(83) Tozuka, Y.; Tashiro, E.; Yonemochi, E.; Oguchi, T.; Yamamoto, K. Solid-State Fluorescence Study of Naphthalene Adsorption on Porous Material. *J. Colloid Interface Sci.* **2002**, *248*, 239–243.

(84) Grimme, S. Do Special Noncovalent Pi-Pi Stacking Interactions Really Exist? *Angew. Chem. Int. Ed. Engl.* **2008**, *47*, 3430–3434.

(85) Walker, M. S. Exciplex Studies. II. Indole and Indole Derivatives. *J. Chem. Phys.* **1967**, *47*, 1020.

(86) Borsarelli, C. D.; Bertolotti, S. G.; Previtali, C. M. Exciplex-Type Behavior and Partition of 3-Substituted Indole Derivatives in Reverse Micelles Made with Benzylhexadecyldimethylammonium Chloride, Water and Benzene. *Photochem. Photobiol.* **2001**, *73*, 97–104.

(87) Samokhvalov, A. Heterogeneous Photocatalytic Reactions of Sulfur Aromatic Compounds. *ChemPhysChem* **2011**, *12*, 2870–2885.

(88) Weljie, a M.; Vogel, H. J. Tryptophan Fluorescence of Calmodulin Binding Domain Peptides Interacting with Calmodulin Containing Unnatural Methionine Analogues. *Protein Eng.* **2000**, *13*, 59–66.

(89) Gonzalez-Béjar, M.; Stiriba, S.-E.; Miranda, M. A.; Pérez-Prieto, J. Positive Photocatalysis of a Diels-Alder Reaction by Quenching of Excited Naphthalene-Indole Charge-Transfer Complex with Cyclohexadiene. *Org. Lett.* **2007**, *9*, 453–456.

(90) Wouters, J.; Quere, L.; Thurston, D. E. *Pharmaceutical Salts and Co-Crystals*; Royal Society of Chemistry: New York, 2011; p. 25.

(91) Karabacak, M.; Cinar, M.; Unal, Z.; Kurt, M. FT-IR, UV Spectroscopic and DFT Quantum Chemical Study on the Molecular Conformation, Vibrational and Electronic Transitions of 2-Aminoterephthalic Acid. *J. Mol. Struct.* **2010**, *982*, 22–27.

(92) Kasha, M. Characterization of Electronic Transitions in Complex Molecules. *Discuss. Faraday Soc.* **1950**, *9*, 14–19.

(93) Klán, P.; Wirz, J. *Photochemistry of Organic Compounds: From Concepts to Practice*; John Wiley & Sons, 2009; p. 40.

(94) Blanco-Brieva, G.; Campos-Martin, J. M.; Al-Zahrani, S. M.; Fierro, J. L. G. Effectiveness of Metal–organic Frameworks for Removal of Refractory Organo-Sulfur Compound Present in Liquid Fuels. *Fuel* **2011**, *90*, 190–197.

(95) Greathouse, J. a; Ockwig, N. W.; Criscenti, L. J.; Guilinger, T. R.; Pohl, P.; Allendorf, M. D. Computational Screening of Metal-Organic Frameworks for Large-Molecule Chemical Sensing. *Phys. Chem. Chem. Phys.* **2010**, *12*, 12621–12629.

(96) Hubbard, S. E.; Hurtubise, R. J. Solid-Matrix Luminescence of Heterocyclic Aromatic Amines in Several New Sugar-Glass Systems. *Talanta* **2007**, *72*, 132–139.

(97) Dai, J.; McKee, M. L.; Samokhvalov, A. Adsorption of Naphthalene and Indole on F300 MOF in Liquid Phase by the Complementary Spectroscopic, Kinetic and DFT Studies. *J. Porous Mater.* in press. DOI: 10.1007/s10934-014-9818-3.